arXiv:2111.12832v3 [physics.chem-ph] 9 Jan 2023

Incorporating Nuclear Quantum Effects in Molecular Dynamics with a Constrained Minimized Energy Surface

Zehua Chen and Yang Yang*

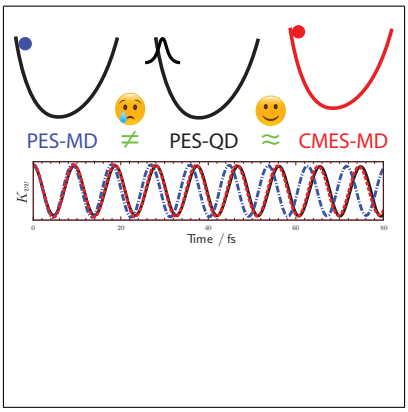
Theoretical Chemistry Institute and Department of Chemistry, University of Wisconsin-Madison, 1101 University Avenue, Madison, Wisconsin 53706, United States

E-mail: yyang222@wisc.edu

Abstract

The accurate incorporation of nuclear quantum effects in large-scale molecular dynamics (MD) simulations remains a significant challenge. Recently, we combined constrained nuclear-electronic orbital (CNEO) theory with classical MD and obtained a new approach (CNEO-MD) that can accurately and efficiently incorporate nuclear quantum effects into classical simulations. In this Letter, we provide the theoretical foundation for CNEO-MD by developing an alternative formulation of the equations of motion for MD. In this new formulation, the expectation values of quantum nuclear positions evolve classically on an effective energy surface that is obtained from a constrained energy minimization procedure when solving for the quantum nuclear wave function, thus enabling the incorporation of nuclear quantum effects in classical MD simulations. For comparison with other existing approaches, we examined a series of model systems and found that this new MD approach is significantly more accurate than the conventional way of performing classical MD, and it also generally outperforms centroid MD and ring-polymer MD in describing vibrations in these model systems.

Graphical TOC Entry



Keywords

nuclear quantum effects, molecular dynamics, multicomponent quantum theory, vibrational spectra

Nuclear quantum effects (NQEs)[1] have a great impact on the structural, thermodynamical, and kinetic properties of a wide range of chemical and biological systems.[2] They usually include zero-point and tunneling effects and are significant when light nuclei, such as hydrogen, are present. The accurate incorporation of NQEs in molecular simulations is important for understanding many fundamental properties but remains a significant challenge for large-scale molecular simulations. For example, the anomalous properties of water are closely related to the NQEs of the complex hydrogen bond network[3,4] and thus cannot be fully explained with conventional classical molecular dynamics (MD) without an accurate inclusion of NQEs.[5]

There have been many theoretical developments in the incorporation of NQEs in molecular simulations. Quantum wave packet dynamics is based on the exact time evolution of a quantum system according to the time-dependent Schrödinger equation and can give theoretical predictions that accurately match experiments.[6–10] Quantum trajectory methods[11] are based on the de Broglie-Bohm formulation of quantum mechanics,[12–17] which attributes quantum effects to the quantum potential, and with a reasonable approximation to the quantum potential, quantum trajectory methods have been applied to many model systems and give accurate results.[18,19] Multicomponent quantum theories[20–26] also include NQEs by simultaneously treating both electrons and key nuclei quantum mechanically, which do not rely on conventional Born-Oppenheimer potential energy surfaces (PESs). Their real-time dynamics simulations.[27–31] can be performed through the quantum time evolution of multicomponent wave functions or density matrices, which have been used to study practical chemical problems, such as proton transfer processes.[32]

Although the aforementioned methods are highly accurate in describing NQEs, they are often hindered by their high computational costs in large molecular or bulk systems. This challenge has been partially addressed using methods based on classical simulations. Some empirical force fields[33] have been used to include NQEs implicitly and have been able to treat hydrogens and deuteriums differently in water.[34] The generalized Langevin equation

thermostat with optimized parameters can also include NQEs and has been applied to obtain several static properties.[35,36] The semiclassical initial value representation (SC-IVR)[37] and its approximate variants[38,39] can also produce accurate time correlation functions with classical simulations. Methods based on the path integral formulation of quantum mechanics[40,41] are most popular for the inclusion of NQEs. Via simultaneous simulation of a set of coupled replicas for a system, path integral molecular dynamics (PIMD)[42,43] can capture NQEs and accurately describe the static properties of the system.[44] Its extensions such as centroid molecular dynamics (CMD)[45,46] and ring-polymer molecular dynamics (RPMD)[47] can describe dynamical properties using approximate time correlation functions. However, while dynamical properties from CMD and RPMD are considerably more accurate than those from conventional MD, challenges still exist with the curvature problem in CMD and spurious frequencies in RPMD. Both of these problems can lead to unreliable vibrational spectra,[48] although several recent developments can mitigate them to some extent, including thermostatted RPMD,[49,50] Matsubara dynamics,[51] and quasicentroid molecular dynamics.[52,53] Furthermore, in contrast with PIMD, which has many techniques developed to make it as efficient as conventional MD,[54–57] currently there are only a limited number of techniques available[58] to accelerate RPMD/CMD simulations other than massive parallelization, and thus, the efficient simulation of dynamical properties remains a challenge.

In this Letter, we present an alternative formulation of the equations of motion for classical molecular simulations, with which NQEs can be described using an effective PES that is in practice approximated by a constrained minimized energy surface (CMES). This formulation serves as the theoretical foundation for our recently developed MD approach based on constrained nuclear-electronic orbital theory (CNEO-MD). For comparison with existing approaches, we examine a series of model systems. We first show that CMES-MD remains exact for the harmonic oscillator model. Then, with a Morse oscillator model and a quartic double-well potential model, we show that CMES-MD is generally much more accurate in describing vibrations and tunneling effects than the conventional way of performing classical

MD and is comparable to or slightly better than CMD and RPMD.

We start with the polar representation of a time-dependent wave function $\psi(\boldsymbol{x},t) = A(\boldsymbol{x},t)\exp(\mathrm{i}S(\boldsymbol{x},t)/\hbar)$, where amplitude part A and phase part S are both real. For the sake of simplicity, we assume in our derivation that there is only one quantum particle, but this formulation can be easily generalized to multiple quantum particle cases if the particles can be assumed to be distinguishable, such as nuclei in regular molecular and bulk systems. Additionally, we will assume that no magnetic field is present, although we note that magnetic fields can be important on some occasions and the corresponding formulation can be explored in the future. With the polar representation, the kinetic energy can be decomposed into two terms

$$\begin{aligned}\langle\hat{T}\rangle(t) = &\int \mathrm{d}\boldsymbol{x} A(\boldsymbol{x},t)\frac{(-\mathrm{i}\hbar\nabla)^2}{2m}A(\boldsymbol{x},t) \\ &+ \frac{1}{2m}\int \mathrm{d}\boldsymbol{x} A^2(\boldsymbol{x},t)[\nabla S(\boldsymbol{x},t)]^2. \end{aligned} \tag{1}$$

The first term is the kinetic energy evaluated with amplitude function A only. Because A is associated with the real space probability density distribution with $\rho(\boldsymbol{x},t) = A^2(\boldsymbol{x},t)$, this term can be perceived as the kinetic energy due to quantum delocalization, or the zero-point kinetic energy. In the second term, the key quantity ∇S is associated with the observable momentum and is related to the momentum field in Bohmian mechanics[12–17] with the definition $\boldsymbol{p}(\boldsymbol{x},t) = \nabla S(\boldsymbol{x},t)$. Because $A^2(\boldsymbol{x},t)$ is the probability density, this term can be viewed as the kinetic energy associated with the observable momentum $\boldsymbol{p}$.

We define the variance of the observable momentum as the variance of the momentum field:

$$\sigma^2_{\boldsymbol{p}}(t) \equiv \int \mathrm{d}\boldsymbol{x} A^2(\boldsymbol{x},t)[\nabla S(\boldsymbol{x},t)]^2 - \langle\hat{\boldsymbol{p}}\rangle^2(t), \tag{2}$$

then the kinetic energy can be further expressed as

$$\langle\hat{T}\rangle(t) = \langle A(t)|\hat{T}|A(t)\rangle + \frac{\langle\hat{\boldsymbol{p}}\rangle^2(t)}{2m} + \frac{\sigma^2_{\boldsymbol{p}}(t)}{2m}. \tag{3}$$

The terms in eq 3 correspond to the zero-point kinetic energy, the classical kinetic energy associated with the expectation value of the observable momentum, and an energy contribution from the variance of the observable momentum field, respectively.

Another way of expressing the kinetic energy is simply $\langle\hat{T}\rangle(t) = \langle\hat{H}\rangle(t) - \langle\hat{V}\rangle(t)$, which can be plugged into the left side of eq 3. Then by taking the time derivative on both sides of the equation, one can simplify it to

$$\frac{\langle\hat{\boldsymbol{p}}\rangle}{m} \cdot \frac{\mathrm{d}\langle\hat{\boldsymbol{p}}\rangle}{\mathrm{d}t} = \left\langle \frac{\partial V}{\partial t} \right\rangle - \frac{\mathrm{d}}{\mathrm{d}t}\langle A(t)|\hat{H}(t)|A(t)\rangle - \frac{\mathrm{d}}{\mathrm{d}t}\frac{\sigma_{\boldsymbol{p}}^2}{2m}. \tag{4}$$

Note that we have used the relationship $\mathrm{d}\langle\hat{H}\rangle(t)/\,\mathrm{d}t = \langle\partial V/\partial t\rangle$ in the derivation. Equation 4 relates the time dependence of momentum to the time dependence of energetic terms. While eq 4 is exact, to make it into an equation of motion that can be practically used in MD simulations, we next proceed with an approximation that builds a connection between quantum states and the classical phase space.

Conventionally, when assuming the potential is slowly varying in space, we have the Ehrenfest theorem that provides a connection between the classical Newtonian dynamics in phase space $(\boldsymbol{X}, \boldsymbol{P})$ and the evolution of quantum expectation values of position and momentum $(\langle\hat{\boldsymbol{x}}\rangle, \langle\hat{\boldsymbol{p}}\rangle)$. Here we build on the same mapping philosophy but instead of assuming the behavior of the potential, we approximate the quantum state as the energy-minimized state for a given phase space point. That is, when the system is at a particular phase space point given by an expectation position and an expectation momentum, i.e., $(\langle\hat{\boldsymbol{x}}\rangle, \langle\hat{\boldsymbol{p}}\rangle) = (\boldsymbol{X}, \boldsymbol{P})$, quantum state $|\psi\rangle$ always adapts to the energy-minimized state for that phase space point. We note that this approximation is an adiabatic approximation and is not trivially justifiable; however, to keep the flow of the derivation, we leave discussions of its applicability as well as limitations for the later part of this Letter.

Under this adiabatic approximation, quantum state $|\psi\rangle$ becomes an explicit function of $(\boldsymbol{X}, \boldsymbol{P})$ and an implicit function of time t, i.e., $|\psi\rangle(\boldsymbol{X}(t), \boldsymbol{P}(t))$. At a particular phase space

point $(\boldsymbol{X}(t), \boldsymbol{P}(t))$ to which the system evolves at time t, the state can be obtained with a constrained energy minimization procedure. The corresponding Lagrangian is

$$\begin{aligned}\mathcal{L} = &\langle\psi|\hat{H}(t)|\psi\rangle + \boldsymbol{f}\cdot(\langle\psi|\hat{\boldsymbol{x}}|\psi\rangle - \boldsymbol{X}(t)) \\ &- \boldsymbol{v}\cdot(\langle\psi|\hat{\boldsymbol{p}}|\psi\rangle - \boldsymbol{P}(t)) - \tilde{E}(\langle\psi|\psi\rangle - 1),\end{aligned} \tag{5}$$

where $\boldsymbol{f}$ is the Lagrange multiplier associated with the expectation position, $\boldsymbol{v}$ is the Lagrange multiplier associated with the expectation momentum, and $\tilde{E}$ is the Lagrange multiplier associated with the wave function normalization. This Lagrangian can be further expressed in terms of A and S by

$$\begin{aligned}\mathcal{L} = &\langle A|\hat{H}(t)|A\rangle + \frac{1}{2m}\int \mathrm{d}\boldsymbol{x} A^2(\nabla S)^2 \\ &+ \boldsymbol{f}\cdot(\langle A|\hat{\boldsymbol{x}}|A\rangle - \boldsymbol{X}(t)) - \boldsymbol{v}\cdot\left(\int \mathrm{d}\boldsymbol{x} A^2\nabla S - \boldsymbol{P}(t)\right) \\ &- \tilde{E}(\langle A|A\rangle - 1).\end{aligned} \tag{6}$$

Making the Lagrangian function stationary with respect to the variation of ∇S and A leads to $A^2(\nabla S/m - \boldsymbol{v}) = 0$ and

$$\left[\hat{H}(t) + \frac{(\nabla S)^2}{2m} + \boldsymbol{f}\cdot\hat{\boldsymbol{x}} - \boldsymbol{v}\cdot\nabla S\right]|A\rangle = \tilde{E}|A\rangle. \tag{7}$$

Further combining these equations with the expectation position constraint, the expectation momentum constraint, and the normalization constraint gives $\boldsymbol{v} = \boldsymbol{P}(t)/m$, $\nabla S(\boldsymbol{x}, t) = m\boldsymbol{v} = \boldsymbol{P}(t)$, and then the eigenvalue equation can be simplified to

$$[\hat{H}(t) + \boldsymbol{f}\cdot\hat{\boldsymbol{x}}]|A\rangle = \left(\tilde{E} + \frac{\boldsymbol{P}^2}{2m}\right)|A\rangle. \tag{8}$$

The eigenvalue $\tilde{E} + \boldsymbol{P}^2/2m$, eigenstate $|A\rangle$, and the Lagrange multiplier $\boldsymbol{f}$ can be solved under the expectation position and normalization constraints for $|A\rangle$. Note that interestingly,

the solution of amplitude function A depends only on the expectation position constraint, and the expectation momentum constraint affects only phase function S.

The fact that the constrained minimization requires ∇S to agree with the momentum expectation value ($\nabla S(\boldsymbol{x}, t) = \boldsymbol{P}(t)$) naturally leads to $\sigma_{\boldsymbol{p}}^2 = 0$ according to the definition in eq 2, and with the quantum state $|A\rangle$ obtained as an explicit function of $\boldsymbol{X}$ and thus an implicit function of t, we can simplify eq 4 into

$$\frac{\langle\hat{\boldsymbol{p}}\rangle}{m} \cdot \frac{\mathrm{d}\langle\hat{\boldsymbol{p}}\rangle}{\mathrm{d}t} \approx -\left\langle \frac{\mathrm{d}A}{\mathrm{d}t}\middle|\hat{H}(t)\middle|A\right\rangle - \left\langle A\middle|\hat{H}(t)\middle|\frac{\mathrm{d}A}{\mathrm{d}t}\right\rangle \tag{9}$$

$$= -\frac{\mathrm{d}\boldsymbol{X}}{\mathrm{d}t} \cdot \Big[\langle\nabla_{\boldsymbol{X}} A|\hat{H}(t)|A\rangle + \langle A|\hat{H}(t)|\nabla_{\boldsymbol{X}} A\rangle\Big] \tag{10}$$

$$= -\frac{\langle\hat{\boldsymbol{p}}\rangle}{m} \cdot \nabla_{\boldsymbol{X}}\langle A|\hat{H}(t)|A\rangle. \tag{11}$$

Note that here we have used $\mathrm{d}\boldsymbol{X}/\,\mathrm{d}t = \mathrm{d}\langle\hat{\boldsymbol{x}}\rangle/\,\mathrm{d}t = \langle\hat{\boldsymbol{p}}\rangle/m$. According to classical mechanics, it is natural to assume that the change in $\langle\hat{\boldsymbol{p}}\rangle$ should have an opposite direction to the energy gradient term ($\nabla_{\boldsymbol{X}}\langle A|\hat{H}(t)|A\rangle$); therefore, the common prefactor $|\langle\hat{\boldsymbol{p}}\rangle|/m$ can be dropped, and we arrive at the final expression

$$\frac{\mathrm{d}\langle\hat{\boldsymbol{p}}\rangle}{\mathrm{d}t} \approx -\nabla_{\boldsymbol{X}}\langle A|\hat{H}(t)|A\rangle \equiv -\nabla_{\boldsymbol{X}} V^{\mathrm{CMES}}(\boldsymbol{X}), \tag{12}$$

where V^{CMES} is the constrained minimized energy surface associated with amplitude part $|A\rangle$. It can also be viewed as an effective potential energy surface that includes not only the potential energy but also the quantum delocalization kinetic energy. Equation 12, together with $\mathrm{d}\langle\hat{\boldsymbol{x}}\rangle/\,\mathrm{d}t = \langle\hat{\boldsymbol{p}}\rangle/m$, forms the equations of motion for CMES-MD. These equations of motion present an alternative way of performing MD simulations but with NQEs incorporated. They are highly similar in structure to Newton's equations used in conventional MD simulations, with the difference that the time evolution is now on the quantum expectation values of positions and momenta rather than the classical ones.

We note that there have been prior works[59–61] that arrived at the same equations of motion within the framework of Feynman's path-integral formulation of quantum mechanics. Within the path-integral framework, the effective potential guides the motion of the ring-polymer centroid and is claimed to be equal to the zero-temperature limit of the centroid potential for CMD.[59,60] Therefore, it has been used to gain insight into the behavior of CMD. In our work presented here, with a formal derivation from the conventional formulation of quantum mechanics, these equations provide a new way of performing classical molecular simulations with the effective potential utilized to guide the classical motion of the quantum expectation values.

Additionally, we note that this formulation serves as the theoretical foundation for our recently published work of CNEO-MD,[62] in which constrained nuclear electronic orbital density functional theory (CNEO-DFT)[63–65] is employed to obtain CMESs for practical molecular systems and used for MD simulations. CNEO-MD is a generalization of CMES-MD when the electronic part is also explicitly considered in the energy minimization procedure. A more detailed derivation of their connections can be found in section S3 of the Supporting Information. With a series of gas phase molecules, we have demonstrated the excellent agreement between the CNEO-MD vibrational spectra and the experimental spectra.[62] Specifically for highly anharmonic O−H and C−H stretching modes, CNEO-MD significantly outperforms conventional DFT-based *ab initio* molecular dynamics, with errors in peak positions reduced by 1 order of magnitude, but at essentially the same computational cost.

For comparison with other existing approaches, herein, we investigate the model systems of a harmonic oscillator, a Morse oscillator and a quartic double-well potential. These model systems are chosen because they have easily accessible exact quantum solutions, avoid errors associated with real systems such as electron correlations, and are affordable for CMD and RPMD simulations. For these model systems, we scan a set of discrete f values in eq 8 to solve for the CMESs. Specifically, for each f, the constrained eigenvalue equation is solved numerically on a grid and the energy as a function of the corresponding nuclear

expectation position is obtained. Afterward, the energies as well as the gradients at arbitrary expectation positions are obtained by cubic spline interpolation during the dynamics simulations. We note that for multidimensional models and practical chemical systems, this way of constructing CMES becomes computationally expensive. Fortunately, in practical systems, CNEO-DFT[63,64] minimizes the total energy of a system with nuclear expectation position constraints and therefore can be used to calculate the CMES on the fly. This work will focus more on building the theoretical foundation and exploring the strengths and limitations of CMES-MD with the help of the simple models.

In our practical model calculations, classical MD and CMES-MD are performed with an in-house python script. Note that throughout the Letter, by conventional MD or classical MD we mean classical molecular simulations based on a Boltzmann sampling of the initial velocity according to the designated temperature and evolving with classical Newtonian equations. We are aware that other methods such as quasi-classical MD[66] and SC-IVR[37–39] that can include zero-point effects in classical simulations exist, but we do not refer to them as classical MD or conventional MD in this Letter. The total simulation time of all conventional MD and CMES-MD simulations is chosen to be 50 ps, and the trajectories are integrated using the velocity-Verlet algorithm with a time step of 0.5 fs. RPMD and CMD simulations on these one-dimensional models are performed with a modified i-PI package.[67] Specifically, a 30 ps PIMD trajectory with 0.1 fs time step is first calculated and used to generate initial configurations for RPMD and CMD. Then RPMD and CMD are performed with a simulation length of 10 ps. For RPMD, the time step is set to 0.1 fs, and for CMD, the time step is 0.003125 fs; the data are recorded every 0.1 fs. For the Morse oscillator model, RPMD and CMD both use 64 beads in simulations with $T = 50$ K, 32 beads in simulations with $T = 300$ K, and 16 beads in simulations with $T = 1500$ K. For the double-well potential model, the corresponding bead numbers are 128 for $T = 50$ K, 64 for $T = 100$ K, and 32 for $T = 1500$ K. We perform 1000 NVE simulations whose initial configurations satisfy the Maxwell-Boltzmann distribution to obtain an NVT ensemble average for classical MD and

CMES-MD; however, this number is reduced to 50 for RPMD and 30 for CMD to limit the computational cost. After the simulations, the trajectories are used to generate correlation functions. In data processing, a correlation depth of 4096 points is used for MD and CMES-MD. For RPMD and CMD, a larger depth of 16384 points is used because of the shorter time step used. Power spectra are obtained via Fourier transforms of the corresponding velocity autocorrelation functions. They are then averaged to obtain the NVT ensemble-averaged power spectra for each method. The intensities of the averaged power spectra are finally adjusted so that they integrate to a number that is proportional to the simulation temperature.

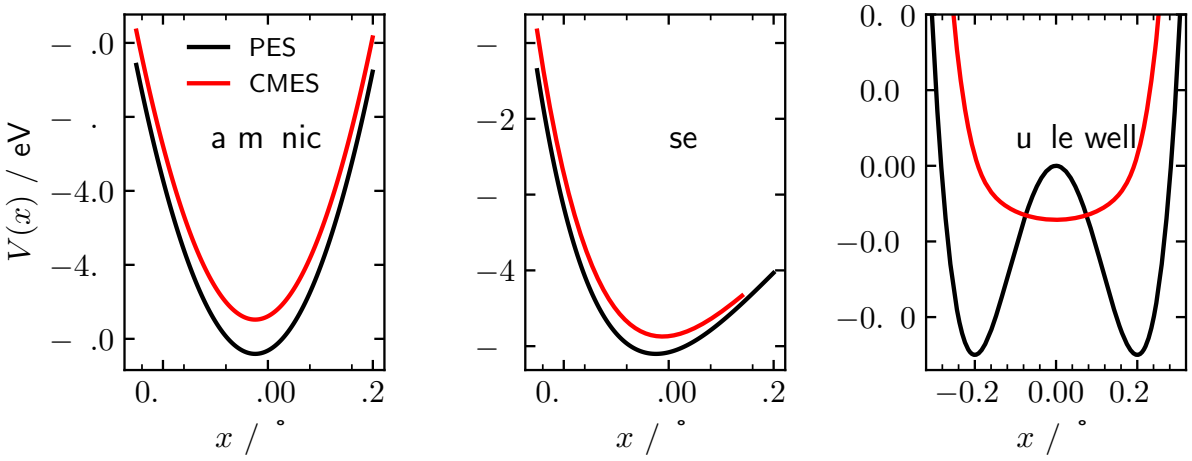


Figure 1: Comparison between the potential energy surface (PES) and constrained minimized energy surface (CMES) for the harmonic oscillator model (left), the Morse oscillator model (middle), and the double-well potential model (right).

The harmonic oscillator $\hat{H} = \hat{p}^2/2m + m\omega^2 (\hat{x} - x_e)^2 /2$ is one particular model for which classical MD gives the same trajectory as the exact quantum theory. CMD and RPMD are also exact for this model system. For CMES-MD, because $\hat{H} + f\hat{x}$ represents the harmonic oscillator with a shifted energy and a shifted position based on the value of f, the constrained minimized energy state $|A\rangle$ for any expectation position $\langle\hat{x}\rangle = X$ is the ground state wave function of $\hat{H}$ shifted to the expectation position $\langle\hat{x}\rangle = X$. Therefore, the corresponding

energy surface as a function of expectation position X is

$$V^{\mathrm{CMES}}(X) = \frac{\hbar\omega}{2} + \frac{1}{2}m\omega^2 \left(X - x_{\mathrm{e}}\right)^2 . \tag{13}$$

This effective potential universally shifts the original harmonic potential upward by $\hbar\omega/2$, which is the zero-point energy for a harmonic oscillator (Figure 1). This result may seem counterintuitive because conventionally ZPE is considered to be a property of the whole energy surface rather than a point-wise property; however, we note that here the ZPE should be more accurately considered as a quantum delocalization energy, which always exists as the quantum wave packet travels through space. Because classical MD produces the exact trajectory on the harmonic potential, the trajectory produced by CMES-MD on V^{CMES} is also exact without any need for numerical tests.

Compared with the harmonic potential, the Morse potential is a better model for chemical bonds with anharmonic effects. Here we use a Morse potential that can mimic the stretch of the O−H radical and perform simulations using classical MD, CMES-MD, RPMD, and CMD. Figure 2 shows the velocity autocorrelation functions and the corresponding power spectra of these methods at three different temperatures. The exact quantum results are used as references, which are obtained from the analytical solution of the Morse potential. Compared with the Kubo-transformed quantum velocity autocorrelation function,[68] classical MD underestimates the period of the correlation function and therefore severely overestimates the vibrational frequency. RPMD and CMD can more accurately describe the correlation function, and their overestimations of the vibrational frequencies are significantly smaller. CMES-MD has the best performance with good agreement with the exact quantum correlation functions and more accurate vibrational frequencies. The good results of CMES-MD at relatively low temperatures are not surprising because CNEO-MD has been known to give accurate vibrational spectra at room temperature,[62] and vibrational frequencies obtained from CNEO-DFT Hessian calculations are also in great agreement with experimental val-

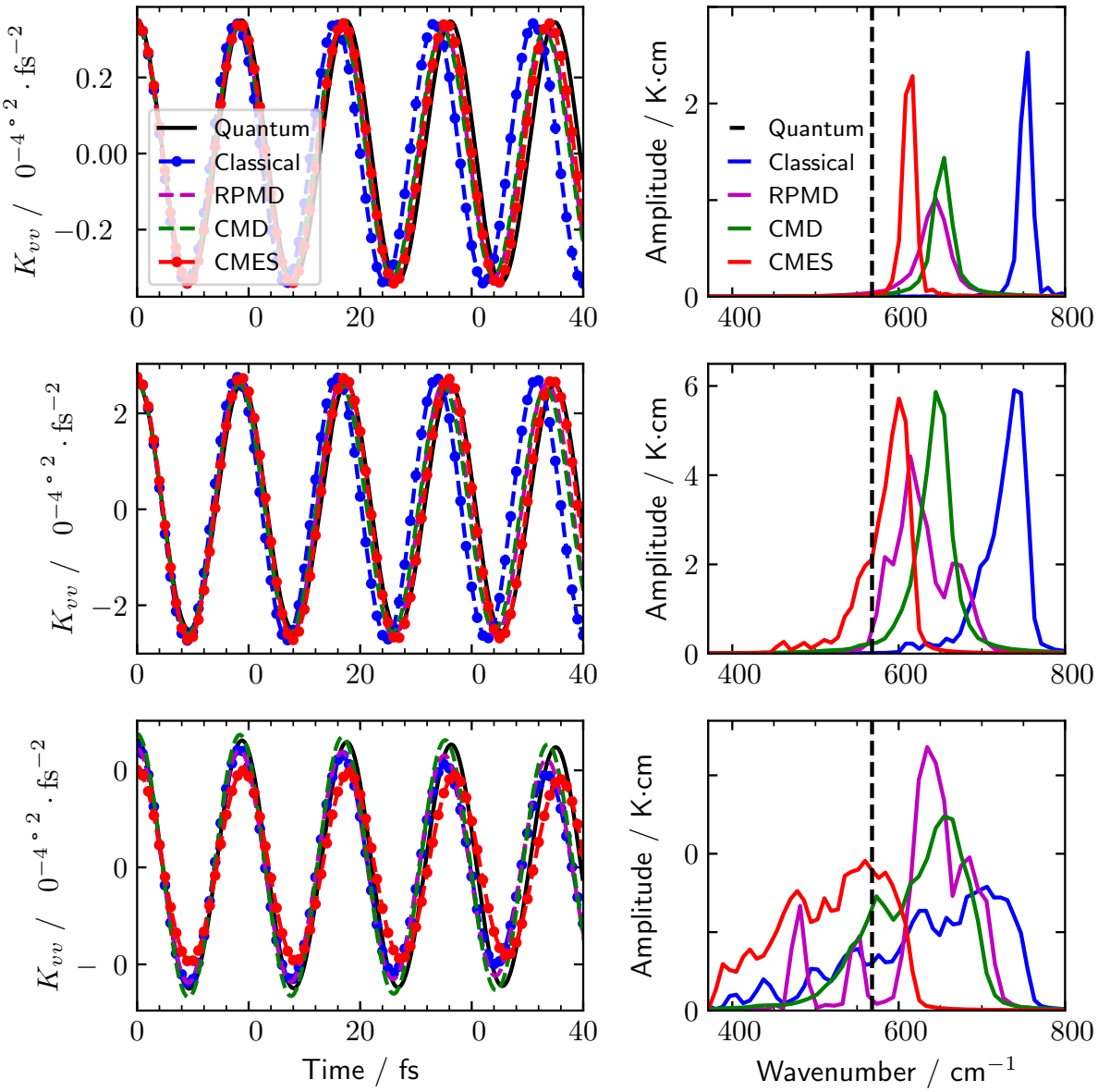


Figure 2: Velocity autocorrelation functions K_{vv} and power spectra of the Morse oscillator mimicking the ^{16}O^{1}H radical at 50 K (top), 300 K (middle) and 1500 K (bottom). The potential form is $V(x) = D_{\mathrm{e}}(\mathrm{e}^{-2\alpha(x-x_{\mathrm{e}})} - 2\mathrm{e}^{-\alpha(x-x_{\mathrm{e}})})$, where $D_{\mathrm{e}} = hc\omega_{\mathrm{e}}^2/4\omega_{\mathrm{e}}\chi_{\mathrm{e}}$ and $\alpha = \sqrt{2\mu hc\omega_{\mathrm{e}}\chi_{\mathrm{e}}/\hbar^2}$. All of the parameters are the same as those used in ref 49, where $\omega_{\mathrm{e}} = 3737.76\,\mathrm{cm}^{-1}$, $\omega_{\mathrm{e}}\chi_{\mathrm{e}} = 84.881\,\mathrm{cm}^{-1}$, and $x_{\mathrm{e}} = 0.96966$ Å. The dashed vertical line represents the exact quantum frequency $3568\,\mathrm{cm}^{-1}$. Two spikes below the quantum frequency in the RPMD 1500 K spectrum are due to insufficient sampling.

ues, indicating a good zero-temperature limit.[65] As the temperature increases, CMES-MD and other simulation methods start to have broader and red-shifted peaks. For this Morse potential, we observe that CMES-MD produces accurate spectra for a temperature range between 50 and 1500 K, suggesting the reliability of CMES-MD in the temperature range in which most chemical and biophysical reactions are performed.

Next we investigate a more challenging double-well potential model, in which quantum tunneling is expected to occur. We use a quartic double-well potential with a 0.125 eV barrier height and a 0.5 Å separation between the potential minima, which can roughly represent the potential energy landscape for a practical proton transfer reaction. As shown in Figure 1, the CMES of this double-well potential is a single well with the minimum located at $X = 0$ due to the symmetrical shape of the ground state wave function with two peaks, whose expectation position is at $\langle \hat{x} \rangle = 0$. As the constrained expectation position deviates from the center, the constrained minimized wave function becomes less symmetrical with more and more excited state character mixed in, thus increasing the energy and forming a single-well effective potential. Note that this picture has also been observed in the literature when investigating the zero-temperature limit of CMD.[59,60]

On this single-well effective potential, the quantum expectation position moves smoothly between left and right as if the barrier does not exist. This is qualitatively in agreement with the quantum picture, in which the wave function can tunnel back and forth through the barrier with a smooth oscillation for the quantum expectation position. This physical picture can be further quantitatively verified by the agreement between the tunneling frequency by CMES-MD and the exact quantum tunneling frequency (Figure 3). At low temperatures, classical MD simulations are all trapped in the local minima of the double well and give position autocorrelation functions that are not vertically centered at zero and a highly overestimated vibrational frequency that is close to the second-order derivative at the local minimum, indicating the failure of classical MD in describing tunneling effects. The two path-integral methods show significant differences in the double-well potential model,

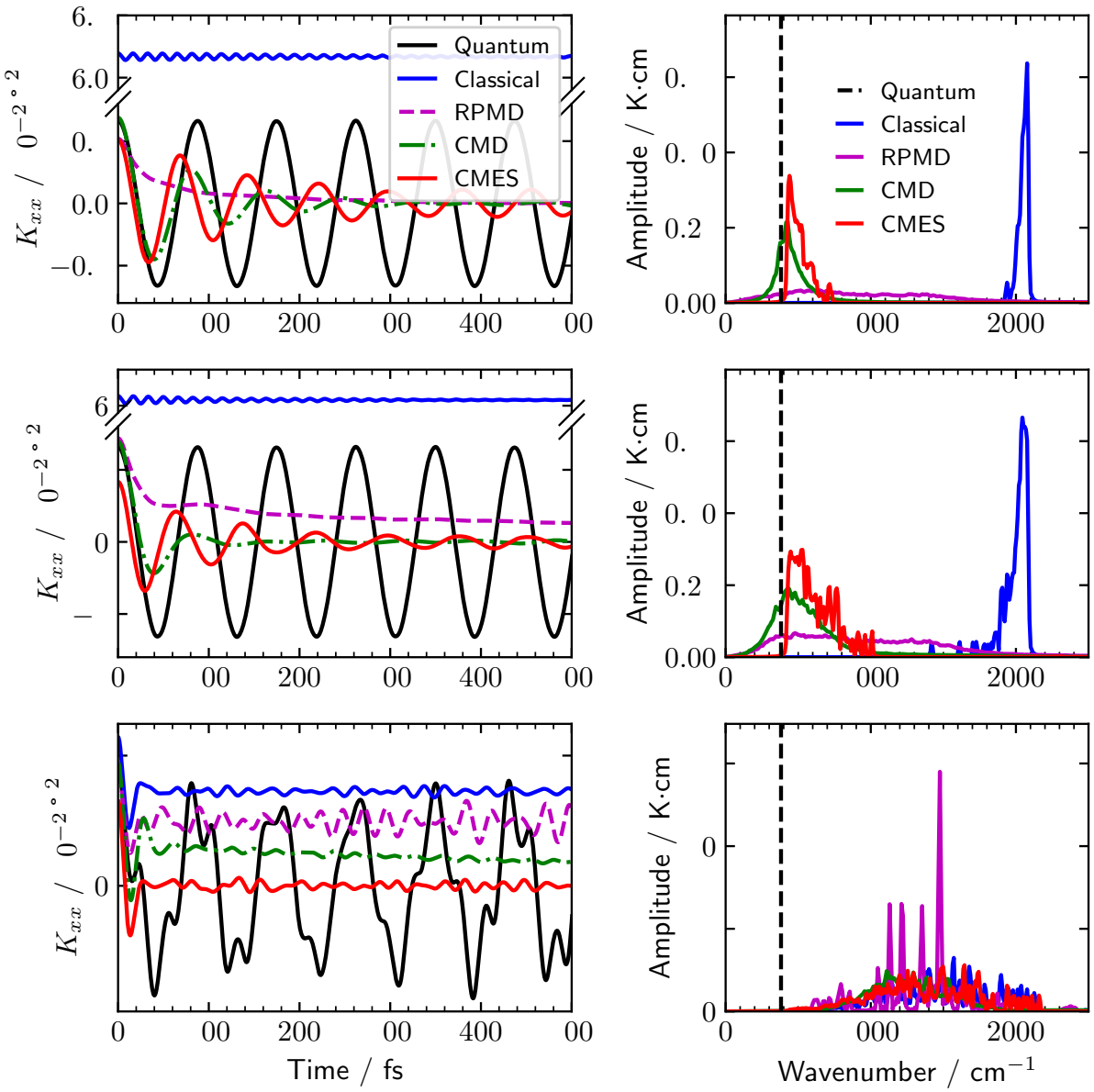


Figure 3: Position autocorrelation function K_{xx} and power spectrum of a proton in the double-well potential at 50 K (top), 100 K (middle) and 1500 K (bottom). The potential form is $V(x) = ax^2 + bx^4$, where $a = -4\,\mathrm{eV/\AA^2}$ and $b = 32\,\mathrm{eV/\AA^4}$. The dashed vertical line represents the exact quantum frequency 382 cm^{-1}. Multiple spikes in the RPMD 1500 K spectrum are due to insufficient sampling.

as CMD gives good autocorrelation functions and predicts a relatively sharp peak with an accurate tunneling frequency, whereas RPMD suffers from a fast decay of the correlation function[69] and a broad peak that smears over a range of nearly 2000 cm^{-1}. CMES-MD is similar to CMD with a slightly overestimated tunneling frequency. As the temperature increases, classical MD shows red-shifts in the peak positions, and CMES-MD and CMD see blue-shifts. At 1500 K, all simulation methods behave very similarly with broad peaks that maximize around 1300-1500 cm^{-1}. All of these results show that CMES-MD performs reasonably well in describing the dynamics in the double-well potential.

We note that quasi-classical MD[66] can be another way to include zero-point effects in classical simulations and can describe well the vibrational frequency of a Morse potential with an appropriate initial energy. However, there are several known issues related to it. For example, it can lead to zero-point energy leakage, where the excess energy of one high-frequency mode may flow to a low-frequency one, sometimes leading to unphysical molecular dissociations.[70,71] Moreover, this method requires the calculation of harmonic frequencies to approximate zero-point energies, which can be problematic if the potential is highly anharmonic. One example is that in the double-well potential, the zero-point energy obtained from the harmonic approximation will be highly inaccurate, and like the classical MD case, the particle may still become trapped on either side of the well if the classical barrier is higher than the zero-point energy. In contrast, CMES-MD and path-integral based methods will not suffer from these problems.

In principle, the effective potential energy surfaces in MD simulations should be temperature-dependent to fully account for nuclear quantum effects. However, although CMES is a temperature-independent effective potential, we observe good performance of CMES-MD over a relatively large temperature range. This suggests that the adiabatic approximation that in essence assumes that the quantum state adapts its wave function to the lowest-energy state for a particular phase space point is reasonable. Nevertheless, it is possible that when the temperature is high and the particle is moving fast, the wave function may not adapt

fast enough to the constrained minimized wave function, thus breaking the adiabatic approximation. Therefore, we expect CMES-MD to be more accurate at low temperatures relative to the mode frequency. Fortunately, for most vibrational modes, room temperature is still considered low temperature, and therefore CMES-MD can be accurate in a good range of temperatures typically investigated by chemical physicists and biophysicists.

Similar to conventional MD, the classical treatment brings not only efficiency but also some limitations. For example, quantum coherence is missing, which is reflected by a decreasing amplitude of the correlation function (Figure 3). Heat capacities will not approach zero when $T \rightarrow 0\,\mathrm{K}$ due to the loss of the energy quantization picture. Furthermore, classical dynamics with distinguishable particles is incapable of capturing the exchange effect, which is important in systems with heavily packed particles, such as in a Bose-Einstein condensate.[72,73] Although detailed studies of these possible limitations are beyond the scope of this work, they are important topics for our future research for better understanding the applicability of CMES-MD. We finally note that due to the similarity between CMES-MD and conventional classical MD, in practical systems, we can expect analytical force field models or even machine-learning force fields (ML-FFs)[74] to be built on the basis of the CMES, which will allow for an even more efficient incorporation of NQEs in MD simulations.

In summary, we provide a new framework for incorporating NQEs into classical molecular simulations. This is achieved through the calculation of the CMES, which serves as the effective potential for classical simulations. In CMES-MD, quantum delocalization and tunneling effects are inherently included and therefore dynamical vibrational frequencies can be accurately described. In simulations of practical systems, CNEO-DFT can be used to obtain the CMES and the resulting CNEO-MD is computationally more efficient than the popular RPMD and CMD methods when *ab initio* PESs are used. It may be further accelerated when combined with modern machine-learning techniques in future developments. As such, CMES/CNEO-MD is a promising new approach to describing NQEs in larger and more complex systems, which will open the door to broader applications.

Acknowledgement

The authors thank David Manolopoulos, Stuart Althorpe, Edwin Sibert, Xi Xu, and James Langford for helpful comments. The authors are grateful for the funding support from the National Science Foundation under Grant 2238473 and from the University of Wisconsin via the Wisconsin Alumni Research Foundation.

Supporting Information Available

Additional details, including detailed derivations for the equations of motion of CMES-MD for single-particle and multiple-particle cases, the connection between CNEO-MD and CMES-MD, and a time propagation test on the performance of CMES-MD.

References

(1) Markland, T. E.; Ceriotti, M. Nuclear Quantum Effects Enter the Mainstream. *Nat. Rev. Chem.* **2018**, *2*, 1–14.

(2) Pereyaslavets, L.; Kurnikov, I.; Kamath, G.; Butin, O.; Illarionov, A.; Leontyev, I.; Olevanov, M.; Levitt, M.; Kornberg, R. D.; Fain, B. On the Importance of Accounting for Nuclear Quantum Effects in Ab Initio Calibrated Force Fields in Biological Simulations. *Proc. Natl. Acad. Sci. U.S.A.* **2018**, *115*, 8878–8882.

(3) Nilsson, A.; Pettersson, L. G. M. The Structural Origin of Anomalous Properties of Liquid Water. *Nat. Commun.* **2015**, *6*, 8998.

(4) Ceriotti, M.; Fang, W.; Kusalik, P. G.; McKenzie, R. H.; Michaelides, A.; Morales, M. A.; Markland, T. E. Nuclear Quantum Effects in Water and Aqueous Systems: Experiment, Theory, and Current Challenges. *Chem. Rev.* **2016**, *116*, 7529–7550.

(5) Zhang, L.; Wang, H.; Car, R.; E, W. Phase Diagram of a Deep Potential Water Model. *Phys. Rev. Lett.* **2021**, *126*, 236001.

(6) Meyer, H. D.; Manthe, U.; Cederbaum, L. S. The Multi-Configurational Time-Dependent Hartree Approach. *Chem. Phys. Lett.* **1990**, *165*, 73–78.

(7) Fleck, J. A.; Morris, J. R.; Feit, M. D. Time-Dependent Propagation of High Energy Laser Beams through the Atmosphere. *Appl. Phys.* **1976**, *10*, 129–160.

(8) Weichman, M. L.; DeVine, J. A.; Babin, M. C.; Li, J.; Guo, L.; Ma, J.; Guo, H.; Neumark, D. M. Feshbach Resonances in the Exit Channel of the F + CH3OH → HF + CH3O Reaction Observed Using Transition-State Spectroscopy. *Nature Chem.* **2017**, *9*, 950–955.

(9) Chen, Z.; Chen, J.; Chen, R.; Xie, T.; Wang, X.; Liu, S.; Wu, G.; Dai, D.; Yang, X.; Zhang, D. H. Reactivity Oscillation in the Heavy–Light–Heavy Cl + CH4 Reaction. *Proc. Natl. Acad. Sci.* **2020**, *117*, 9202–9207.

(10) Chen, W.; Wang, R.; Yuan, D.; Zhao, H.; Luo, C.; Tan, Y.; Li, S.; Zhang, D. H.; Wang, X.; Sun, Z. et al. Quantum Interference between Spin-Orbit Split Partial Waves in the F + HD → HF + D Reaction. *Science* **2021**, *371*, 936–940.

(11) Lopreore, C. L.; Wyatt, R. E. Quantum Wave Packet Dynamics with Trajectories. *Phys. Rev. Lett.* **1999**, *82*, 5190–5193.

(12) De Broglie, L. Sur la possibilité de relier les phénomenes d'interférence et de diffractiona la théorie des quanta de lumiere. *Comptes Rendus* **1926**, *183*, 447–448.

(13) De Broglie, L. La structure atomique de la matière et du rayonnement et la Mécanique ondulatoire. *CR Acad. Sci. Paris* **1927**, *184*, 273–274.

(14) Madelung, E. Quantentheorie in hydrodynamischer Form. *Z. Physik* **1927**, *40*, 322–326.

(15) Bohm, D. A Suggested Interpretation of the Quantum Theory in Terms of "Hidden" Variables. I. *Phys. Rev.* **1952**, *85*, 166–179.

(16) Bohm, D. A Suggested Interpretation of the Quantum Theory in Terms of "Hidden" Variables. II. *Phys. Rev.* **1952**, *85*, 180–193.

(17) Schleich, W. P.; Greenberger, D. M.; Kobe, D. H.; Scully, M. O. Schrödinger equation revisited. *Proc. Natl. Acad. Sci. U.S.A.* **2013**, *110*, 5374–5379.

(18) Garashchuk, S.; Rassolov, V. A. Quantum Dynamics with Bohmian Trajectories: Energy Conserving Approximation to the Quantum Potential. *Chem. Phys. Lett.* **2003**, *376*, 358–363.

(19) Garashchuk, S.; Rassolov, V. Energy Conserving Approximations to the Quantum Potential: Dynamics with Linearized Quantum Force. *J. Chem. Phys.* **2004**, *120*, 1181–1190.

(20) Thomas, I. L. Protonic Structure of Molecules. I. Ammonia Molecules. *Phys. Rev.* **1969**, *185*, 90–94.

(21) Capitani, J. F.; Nalewajski, R. F.; Parr, R. G. Non-Born-Oppenheimer Density Functional Theory of Molecular Systems. *J. Chem. Phys.* **1982**, *76*, 568–573.

(22) Tachikawa, M.; Mori, K.; Nakai, H.; Iguchi, K. An Extension of Ab Initio Molecular Orbital Theory to Nuclear Motion. *Chem. Phys. Lett.* **1998**, *290*, 437–442.

(23) Kreibich, T.; Gross, E. K. U. Multicomponent Density-Functional Theory for Electrons and Nuclei. *Phys. Rev. Lett.* **2001**, *86*, 2984–2987.

(24) Webb, S. P.; Iordanov, T.; Hammes-Schiffer, S. Multiconfigurational Nuclear-Electronic Orbital Approach: Incorporation of Nuclear Quantum Effects in Electronic Structure Calculations. *J. Chem. Phys.* **2002**, *117*, 4106–4118.

(25) Ishimoto, T.; Tachikawa, M.; Nagashima, U. Review of Multicomponent Molecular Orbital Method for Direct Treatment of Nuclear Quantum Effect. *Int. J. Quantum Chem.* **2009**, *109*, 2677–2694.

(26) Pavošević, F.; Culpitt, T.; Hammes-Schiffer, S. Multicomponent Quantum Chemistry: Integrating Electronic and Nuclear Quantum Effects via the Nuclear-Electronic Orbital Method. *Chem. Rev.* **2020**, *120*, 4222–4253.

(27) Abedi, A.; Maitra, N. T.; Gross, E. K. U. Exact Factorization of the Time-Dependent Electron-Nuclear Wave Function. *Phys. Rev. Lett.* **2010**, *105*, 123002.

(28) Suzuki, Y.; Abedi, A.; Maitra, N. T.; Gross, E. K. U. Laser-Induced Electron Localization in H_2^+: Mixed Quantum-Classical Dynamics Based on the Exact Time-Dependent Potential Energy Surface. *Phys. Chem. Chem. Phys.* **2015**, *17*, 29271–29280.

(29) Zhao, L.; Tao, Z.; Pavošević, F.; Wildman, A.; Hammes-Schiffer, S.; Li, X. Real-Time Time-Dependent Nuclear-Electronic Orbital Approach: Dynamics beyond the Born-Oppenheimer Approximation. *J. Phys. Chem. Lett.* **2020**, *11*, 4052–4058.

(30) Zhao, L.; Wildman, A.; Tao, Z.; Schneider, P.; Hammes-Schiffer, S.; Li, X. Nuclear-Electronic Orbital Ehrenfest Dynamics. *J. Chem. Phys.* **2020**, *153*, 224111.

(31) Tao, Z.; Yu, Q.; Roy, S.; Hammes-Schiffer, S. Direct Dynamics with Nuclear–Electronic Orbital Density Functional Theory. *Acc. Chem. Res.* **2021**, *54*, 4131–4141.

(32) Zhao, L.; Wildman, A.; Pavošević, F.; Tully, J. C.; Hammes-Schiffer, S.; Li, X. Excited State Intramolecular Proton Transfer with Nuclear-Electronic Orbital Ehrenfest Dynamics. *J. Phys. Chem. Lett.* **2021**, *12*, 3497–3502.

(33) Grigera, J. R. An Effective Pair Potential for Heavy Water. *J. Chem. Phys.* **2001**, *114*, 8064–8067.

(34) Ben Abu, N.; Mason, P. E.; Klein, H.; Dubovski, N.; Ben Shoshan-Galeczki, Y.; Malach, E.; Pražienková, V.; Maletínská, L.; Tempra, C.; Chamorro, V. C. et al. Sweet Taste of Heavy Water. *Commun. Biol.* **2021**, *4*, 1–10.

(35) Ceriotti, M.; Bussi, G.; Parrinello, M. Langevin Equation with Colored Noise for Constant-Temperature Molecular Dynamics Simulations. *Phys. Rev. Lett.* **2009**, *102*, 020601.

(36) Ceriotti, M.; Bussi, G.; Parrinello, M. Nuclear Quantum Effects in Solids Using a Colored-Noise Thermostat. *Phys. Rev. Lett.* **2009**, *103*, 030603.

(37) Wang, H.; Sun, X.; Miller, W. H. Semiclassical Approximations for the Calculation of Thermal Rate Constants for Chemical Reactions in Complex Molecular Systems. *J. Chem. Phys.* **1998**, *108*, 9726–9736.

(38) Sun, X.; Wang, H.; Miller, W. H. Semiclassical Theory of Electronically Nonadiabatic Dynamics: Results of a Linearized Approximation to the Initial Value Representation. *J. Chem. Phys.* **1998**, *109*, 7064–7074.

(39) Liu, J.; Miller, W. H. A Simple Model for the Treatment of Imaginary Frequencies in Chemical Reaction Rates and Molecular Liquids. *J. Chem. Phys.* **2009**, *131*, 074113.

(40) Feynman, R. P.; Hibbs, A. R.; Styer, D. F. *Quantum Mechanics and Path Integrals*; Courier Corp., 2010.

(41) Feynman, R. P. *Statistical Mechanics*; Addison-Wesley, 1972.

(42) Berne, B. J.; Ciccotti, G.; Coker, D. F. *Classical and Quantum Dynamics in Condensed Phase Simulations: Proceedings of the International School of Physics*; World Scientific, 1998.

(43) Tuckerman, M. E. Path integration via molecular dynamics. *Quantum Simulations of Complex Many-Body Systems: From Theory to Algorithms* **2002**, *Vol. 10*, p 269.

(44) Herrero, C. P.; Ramírez, R. Path-Integral Simulation of Solids. *J. Phys.: Condens. Matter* **2014**, *26*, 233201.

(45) Cao, J.; Voth, G. A. The Formulation of Quantum Statistical Mechanics Based on the Feynman Path Centroid Density. II. Dynamical Properties. *J. Chem. Phys.* **1994**, *100*, 5106–5117.

(46) Jang, S.; Voth, G. A. A Derivation of Centroid Molecular Dynamics and Other Approximate Time Evolution Methods for Path Integral Centroid Variables. *J. Chem. Phys.* **1999**, *111*, 2371–2384.

(47) Craig, I. R.; Manolopoulos, D. E. Quantum Statistics and Classical Mechanics: Real Time Correlation Functions from Ring Polymer Molecular Dynamics. *J. Chem. Phys.* **2004**, *121*, 3368–3373.

(48) Witt, A.; Ivanov, S. D.; Shiga, M.; Forbert, H.; Marx, D. On the Applicability of Centroid and Ring Polymer Path Integral Molecular Dynamics for Vibrational Spectroscopy. *J. Chem. Phys.* **2009**, *130*, 194510.

(49) Rossi, M.; Ceriotti, M.; Manolopoulos, D. E. How to Remove the Spurious Resonances from Ring Polymer Molecular Dynamics. *J. Chem. Phys.* **2014**, *140*, 234116.

(50) Rossi, M.; Kapil, V.; Ceriotti, M. Fine Tuning Classical and Quantum Molecular Dynamics Using a Generalized Langevin Equation. *J. Chem. Phys.* **2018**, *148*, 102301.

(51) Hele, T. J. H.; Willatt, M. J.; Muolo, A.; Althorpe, S. C. Boltzmann-Conserving Classical Dynamics in Quantum Time-Correlation Functions: "Matsubara Dynamics". *J. Chem. Phys.* **2015**, *142*, 134103.

(52) Haggard, C.; Sadhasivam, V. G.; Trenins, G.; Althorpe, S. C. Testing the Quasicentroid Molecular Dynamics Method on Gas-Phase Ammonia. *J. Chem. Phys.* **2021**, *155*, 174120.

(53) Fletcher, T.; Zhu, A.; Lawrence, J. E.; Manolopoulos, D. E. Fast Quasi-Centroid Molecular Dynamics. *J. Chem. Phys.* **2021**, *155*, 231101.

(54) Kapil, V.; VandeVondele, J.; Ceriotti, M. Accurate Molecular Dynamics and Nuclear Quantum Effects at Low Cost by Multiple Steps in Real and Imaginary Time: Using Density Functional Theory to Accelerate Wavefunction Methods. *J. Chem. Phys.* **2016**, *144*, 054111.

(55) Marsalek, O.; Markland, T. E. Ab Initio Molecular Dynamics with Nuclear Quantum Effects at Classical Cost: Ring Polymer Contraction for Density Functional Theory. *J. Chem. Phys.* **2016**, *144*, 054112.

(56) Uhl, F.; Marx, D.; Ceriotti, M. Accelerated Path Integral Methods for Atomistic Simulations at Ultra-Low Temperatures. *J. Chem. Phys.* **2016**, *145*, 054101.

(57) Xue, Y.; Wang, J.-N.; Hu, W.; Zheng, J.; Li, Y.; Pan, X.; Mo, Y.; Shao, Y.; Wang, L.; Mei, Y. Affordable Ab Initio Path Integral for Thermodynamic Properties via Molecular Dynamics Simulations Using Semiempirical Reference Potential. *J. Phys. Chem. A* **2021**, *125*, 10677–10685.

(58) Gui, X.; Fan, W.; Sun, J.; Li, Y. New Stable and Fast Ring-Polymer Molecular Dynamics for Calculating Bimolecular Rate Coefficients with an Example of OH + CH4. *J. Chem. Theory Comput.* **2022**, *18*, 5203–5212.

(59) Ramírez, R.; López-Ciudad, T.; Noya, J. C. Feynman Effective Classical Potential in the Schrödinger Formulation. *Phys. Rev. Lett.* **1998**, *81*, 3303–3306.

(60) Ramírez, R.; López-Ciudad, T. The Schrödinger Formulation of the Feynman Path Centroid Density. *J. Chem. Phys.* **1999**, *111*, 3339–3348.

(61) Ramírez, R.; López-Ciudad, T. Phase-Space Formulation of Thermodynamic and Dynamical Properties of Quantum Particles. *Phys. Rev. Lett.* **1999**, *83*, 4456–4459.

(62) Xu, X.; Chen, Z.; Yang, Y. Molecular Dynamics with Constrained Nuclear Electronic Orbital Density Functional Theory: Accurate Vibrational Spectra from Efficient Incorporation of Nuclear Quantum Effects. *J. Am. Chem. Soc.* **2022**, *144*, 4039–4046.

(63) Xu, X.; Yang, Y. Full-Quantum Descriptions of Molecular Systems from Constrained Nuclear-Electronic Orbital Density Functional Theory. *J. Chem. Phys.* **2020**, *153*, 074106.

(64) Xu, X.; Yang, Y. Constrained Nuclear-Electronic Orbital Density Functional Theory: Energy Surfaces with Nuclear Quantum Effects. *J. Chem. Phys.* **2020**, *152*, 084107.

(65) Xu, X.; Yang, Y. Molecular Vibrational Frequencies from Analytic Hessian of Constrained Nuclear-Electronic Orbital Density Functional Theory. *J. Chem. Phys.* **2021**, *154*, 244110.

(66) Karplus, M.; Porter, R. N.; Sharma, R. D. Dynamics of Reactive Collisions: The H +H2 Exchange Reaction. *J. Chem. Phys.* **1964**, *40*, 2033–2034.

(67) Ceriotti, M.; More, J.; Manolopoulos, D. E. I-PI: A Python Interface for Ab Initio Path Integral Molecular Dynamics Simulations. *Comput. Phys. Commun.* **2014**, *185*, 1019–1026.

(68) Kubo, R. Statistical-Mechanical Theory of Irreversible Processes. I. General Theory and Simple Applications to Magnetic and Conduction Problems. *J. Phys. Soc. Jpn.* **1957**, *12*, 570–586.

(69) Smith, K. K. G.; Poulsen, J. A.; Nyman, G.; Rossky, P. J. A New Class of Ensemble Conserving Algorithms for Approximate Quantum Dynamics: Theoretical Formulation and Model Problems. *J. Chem. Phys.* **2015**, *142*, 244112.

(70) Guo, Y.; Thompson, D. L.; Sewell, T. D. Analysis of the Zero-point Energy Problem in Classical Trajectory Simulations. *J. Chem. Phys.* **1996**, *104*, 576–582.

(71) Ben-Nun, M.; Levine, R. D. On the Zero Point Energy in Classical Trajectory Computations. *J. Chem. Phys.* **1996**, *105*, 8136–8141.

(72) Einstein, A. *Albert Einstein: Akademie-Vorträge*; John Wiley & Sons, Ltd, 2005; pp 245–257.

(73) Bose, Plancks Gesetz und Lichtquantenhypothese. *Z. Physik* **1924**, *26*, 178–181.

(74) Unke, O. T.; Chmiela, S.; Sauceda, H. E.; Gastegger, M.; Poltavsky, I.; Schütt, K. T.; Tkatchenko, A.; Müller, K.-R. Machine Learning Force Fields. *Chem. Rev.* **2021**, *121*, 10142–10186.

arXiv:2111.12832v3 [physics.chem-ph] 9 Jan 2023

Supporting Information: Incorporating Nuclear Quantum Effects in Molecular Dynamics with a Constrained Minimized Energy Surface

Zehua Chen and Yang Yang*

Theoretical Chemistry Institute and Department of Chemistry, University of Wisconsin-Madison, 1101 University Avenue, Madison, Wisconsin 53706, United States

E-mail: yyang222@wisc.edu

Here we present the detailed derivation for the equations of motion of CMES-MD for single-particle and multiple-particle cases, as well as its connection with CNEO-MD. In the last section, as suggested by a reviewer, we show a test on the performance of CMES-MD based on trajectory analysis.

S1 Detailed derivation for equations of motion of CMES-MD

In this section, for simplicity, we assume that there is only one quantum particle. However, the extension to the multi-particle case is straightforward if the particles can be assumed to be distinguishable, which will be shown in section S2.

S1.1 Decomposition of kinetic energy

We start with the polar representation of a time-dependent wave function

$$\psi(\boldsymbol{x},t) = A(\boldsymbol{x},t)\exp\left(\frac{\mathrm{i}}{\hbar}S(\boldsymbol{x},t)\right), \tag{S1}$$

where A and S are both real functions. Then we can evaluate a few quantities in terms of A and S.

The expectation value of the position operator $\langle\hat{\boldsymbol{x}}\rangle(t)$ is

$$\langle\hat{\boldsymbol{x}}\rangle(t) = \langle\psi|\hat{\boldsymbol{x}}|\psi\rangle = \int \mathrm{d}\boldsymbol{x}|\psi(\boldsymbol{x},t)|^2\boldsymbol{x} = \int \mathrm{d}\boldsymbol{x}A^2(\boldsymbol{x},t)\boldsymbol{x}, \tag{S2}$$

The expectation value of the momentum operator is

$$\langle\hat{\boldsymbol{p}}\rangle(t) = \langle\psi|\hat{\boldsymbol{p}}|\psi\rangle = -\mathrm{i}\hbar\int \mathrm{d}\boldsymbol{x}\psi^*(\boldsymbol{x},t)\nabla\psi(\boldsymbol{x},t) \tag{S3}$$

$$= -\mathrm{i}\hbar\int \mathrm{d}\boldsymbol{x}A(\boldsymbol{x},t)\exp\left(-\frac{\mathrm{i}}{\hbar}S(\boldsymbol{x},t)\right)\nabla\left[A(\boldsymbol{x},t)\exp\left(\frac{\mathrm{i}}{\hbar}S(\boldsymbol{x},t)\right)\right] \tag{S4}$$

$$= -\mathrm{i}\hbar \int \mathrm{d}\boldsymbol{x} A(\boldsymbol{x},t)\nabla A(\boldsymbol{x},t) + \int \mathrm{d}\boldsymbol{x} A^2(\boldsymbol{x},t)\nabla S(\boldsymbol{x},t) \tag{S5}$$

$$= -\frac{\mathrm{i}\hbar}{2} \int \mathrm{d}\boldsymbol{x} \nabla A^2(\boldsymbol{x},t) + \int \mathrm{d}\boldsymbol{x} A^2(\boldsymbol{x},t)\nabla S(\boldsymbol{x},t) \tag{S6}$$

$$= \int \mathrm{d}\boldsymbol{x} A^2(\boldsymbol{x},t)\nabla S(\boldsymbol{x},t). \tag{S7}$$

Note that $\int \mathrm{d}\boldsymbol{x}\nabla A^2(\boldsymbol{x},t)$ is zero because the wave function needs to vanish at infinity.

Using the time-dependent Schrödinger equation

$$\mathrm{i}\hbar\frac{\partial}{\partial t}\psi(\boldsymbol{x},t) = \hat{H}(t)\psi(\boldsymbol{x},t), \tag{S8}$$

where the Hamiltonian operator consists of kinetic energy part and potential energy part

$$\hat{H}(t) = -\frac{\hbar^2}{2m}\nabla^2 + V(\boldsymbol{x},t). \tag{S9}$$

The first equation of the Ehrenfest theorem can be derived:

$$\frac{\mathrm{d}\langle\hat{\boldsymbol{x}}\rangle(t)}{\mathrm{d}t} = \int \mathrm{d}\boldsymbol{x} \left[\frac{\partial\psi^*(\boldsymbol{x},t)}{\partial t}\psi(\boldsymbol{x},t) + \psi^*(\boldsymbol{x},t)\frac{\partial\psi(\boldsymbol{x},t)}{\partial t}\right]\boldsymbol{x} \tag{S10}$$

$$= -\frac{\mathrm{i}}{\hbar}\int \mathrm{d}\boldsymbol{x}[-\psi(\boldsymbol{x},t)\hat{H}\psi^*(\boldsymbol{x},t) + \psi^*(\boldsymbol{x},t)\hat{H}\psi(\boldsymbol{x},t)]\boldsymbol{x} \tag{S11}$$

$$= \frac{\mathrm{i}\hbar}{2m}\int \mathrm{d}\boldsymbol{x}[-\psi(\boldsymbol{x},t)\nabla^2\psi^*(\boldsymbol{x},t) + \psi^*(\boldsymbol{x},t)\nabla^2\psi(\boldsymbol{x},t)]\boldsymbol{x} \tag{S12}$$

$$= \frac{\mathrm{i}\hbar}{2m}\int \mathrm{d}\boldsymbol{x}[-\boldsymbol{x}\psi(\boldsymbol{x},t)\nabla^2\psi^*(\boldsymbol{x},t) + \boldsymbol{x}\psi^*(\boldsymbol{x},t)\nabla^2\psi(\boldsymbol{x},t)] \tag{S13}$$

$$= \frac{\mathrm{i}\hbar}{2m}\int \mathrm{d}\boldsymbol{x}\nabla[\boldsymbol{x}\psi(\boldsymbol{x},t)]\nabla\psi^*(\boldsymbol{x},t) - \nabla[\boldsymbol{x}\psi^*(\boldsymbol{x},t)]\nabla\psi(\boldsymbol{x},t) \tag{S14}$$

$$= \frac{\mathrm{i}\hbar}{2m}\int \mathrm{d}\boldsymbol{x}\big[\boldsymbol{x}\nabla\psi(\boldsymbol{x},t)\nabla\psi^*(\boldsymbol{x},t) + \psi(\boldsymbol{x},t)\nabla\psi^*(\boldsymbol{x},t)$$

$$- \boldsymbol{x}\nabla\psi^*(\boldsymbol{x},t)\nabla\psi(\boldsymbol{x},t) - \psi^*(\boldsymbol{x},t)\nabla\psi(\boldsymbol{x},t)\big] \tag{S15}$$

$$= \frac{\mathrm{i}\hbar}{2m}\int \mathrm{d}\boldsymbol{x}[\psi(\boldsymbol{x},t)\nabla\psi^*(\boldsymbol{x},t) - \psi^*(\boldsymbol{x},t)\nabla\psi(\boldsymbol{x},t)] \tag{S16}$$

$$= \frac{1}{2m}\int \mathrm{d}\boldsymbol{x}[\psi(\boldsymbol{x},t)(\mathrm{i}\hbar\nabla)\psi^*(\boldsymbol{x},t) + \psi^*(\boldsymbol{x},t)(-\mathrm{i}\hbar\nabla)\psi(\boldsymbol{x},t)] \tag{S17}$$

$$= \frac{1}{m}\int \mathrm{d}\boldsymbol{x} A^2(\boldsymbol{x},t)\nabla S(\boldsymbol{x},t) \tag{S18}$$

$$= \frac{\langle \hat{\boldsymbol{p}} \rangle(t)}{m}, \tag{S19}$$

where the potential parts of the Hamiltonian cancel, and the we have used again the requirement that the wave function needs to vanish at infinity.

Now we derive eq 1 in the main paper, which is the kinetic energy in terms of A and S:

$$\langle \hat{T} \rangle(t) = \frac{\langle \hat{\boldsymbol{p}}^2 \rangle(t)}{2m} \tag{S20}$$

$$= -\frac{\hbar^2}{2m} \int \mathrm{d}\boldsymbol{x} \psi^*(\boldsymbol{x}, t) \nabla^2 \psi(\boldsymbol{x}, t) \tag{S21}$$

$$= \frac{\hbar^2}{2m} \int \mathrm{d}\boldsymbol{x} [\nabla \psi^*(\boldsymbol{x}, t)] \cdot [\nabla \psi(\boldsymbol{x}, t)] \tag{S22}$$

$$= \frac{\hbar^2}{2m} \int \mathrm{d}\boldsymbol{x} \left\{ \nabla \left[A(\boldsymbol{x}, t) \exp\left(-\frac{\mathrm{i}}{\hbar} S(\boldsymbol{x}, t) \right) \right] \right\} \cdot \left\{ \nabla \left[A(\boldsymbol{x}, t) \exp\left(\frac{\mathrm{i}}{\hbar} S(\boldsymbol{x}, t) \right) \right] \right\} \tag{S23}$$

$$= \frac{\hbar^2}{2m} \int \mathrm{d}\boldsymbol{x} \left\{ [\nabla A(\boldsymbol{x}, t)] \exp\left(-\frac{\mathrm{i}}{\hbar} S(\boldsymbol{x}, t) \right) - \frac{\mathrm{i}}{\hbar} [\nabla S(\boldsymbol{x}, t)] A(\boldsymbol{x}, t) \exp\left(-\frac{\mathrm{i}}{\hbar} S(\boldsymbol{x}, t) \right) \right\} \cdot \left\{ [\nabla A(\boldsymbol{x}, t)] \exp\left(\frac{\mathrm{i}}{\hbar} S(\boldsymbol{x}, t) \right) + \frac{\mathrm{i}}{\hbar} [\nabla S(\boldsymbol{x}, t)] A(\boldsymbol{x}, t) \exp\left(\frac{\mathrm{i}}{\hbar} S(\boldsymbol{x}, t) \right) \right\} \tag{S24}$$

$$= \frac{\hbar^2}{2m} \int \mathrm{d}\boldsymbol{x} [\nabla A(\boldsymbol{x}, t)]^2 + \frac{1}{2m} \int \mathrm{d}\boldsymbol{x} A^2(\boldsymbol{x}, t) [\nabla S(\boldsymbol{x}, t)]^2 \tag{S25}$$

$$= \int \mathrm{d}\boldsymbol{x} A(\boldsymbol{x}, t) \frac{(-\mathrm{i}\hbar\nabla)^2}{2m} A(\boldsymbol{x}, t) + \frac{1}{2m} \int \mathrm{d}\boldsymbol{x} A^2(\boldsymbol{x}, t) [\nabla S(\boldsymbol{x}, t)]^2. \tag{S26}$$

Here the integration by parts is used again with wave function boundary conditions. We can see that the kinetic energy can be decomposed into two parts.

The first part is only about amplitude A, which roughly depends on how localized A is, and is the zero-point kinetic energy if phase part S does not exist.

The second part is directly about ∇S, which is related to the observable momentum. In fact, with the definition of the momentum field $p(\boldsymbol{x}, t) \equiv \nabla S(\boldsymbol{x}, t)$ according to Bohmian mechanics,[1–6] this term can be written as

$$\frac{1}{2m} \int \mathrm{d}\boldsymbol{x} A^2(\boldsymbol{x}, t) [\nabla S(\boldsymbol{x}, t)]^2 = \frac{\langle \hat{\boldsymbol{p}} \rangle^2(t)}{2m} + \frac{\sigma_{\boldsymbol{p}}^2(t)}{2m}, \tag{S27}$$

where $\sigma^2_{\boldsymbol{p}}(t)$ is the variance of the observable momentum field that is defined as

$$\sigma^2_{\boldsymbol{p}}(t) \equiv \int \mathrm{d}\boldsymbol{x} A^2(\boldsymbol{x},t)[\nabla S(\boldsymbol{x},t)]^2 - \langle\hat{\boldsymbol{p}}\rangle^2(t). \tag{S28}$$

In this way, the total kinetic energy can be written as

$$\langle\hat{T}\rangle(t) = \langle A(t)|\hat{T}|A(t)\rangle + \frac{\langle\hat{\boldsymbol{p}}\rangle^2(t)}{2m} + \frac{\sigma^2_{\boldsymbol{p}}(t)}{2m}. \tag{S29}$$

We can see that with this decomposition, the total kinetic energy is the sum of: (1) the zero-point kinetic energy from the delocalized amplitude part, (2) the classical kinetic energy from the observable momentum, and (3) the variance of the observable momentum field.

S1.2 Equations of motion

Equation S19 gives the $\mathrm{d}\boldsymbol{x}/\,\mathrm{d}t$ part of equation of motion. In order to get the $\mathrm{d}\boldsymbol{p}/\,\mathrm{d}t$ part of the equations of motion, we start with the following energy identity,

$$\langle\hat{H}\rangle = \langle\hat{T}\rangle + \langle\hat{V}\rangle. \tag{S30}$$

Then taking the time derivative on each term gives

$$\frac{\mathrm{d}}{\mathrm{d}t}\langle\hat{T}\rangle = \frac{\mathrm{d}}{\mathrm{d}t}\langle\hat{H}\rangle - \frac{\mathrm{d}}{\mathrm{d}t}\langle\hat{V}\rangle \tag{S31}$$

$$= \langle\frac{\partial\hat{H}}{\partial t}\rangle - \frac{\mathrm{d}}{\mathrm{d}t}\langle\hat{V}\rangle \tag{S32}$$

$$= \langle\frac{\partial V(\boldsymbol{x},t)}{\partial t}\rangle - \frac{\mathrm{d}}{\mathrm{d}t}\langle\hat{V}\rangle. \tag{S33}$$

Here the first step has used the time-dependent Schrödinger equation, and the second step has used that the kinetic energy operator is not time-dependent. We note that in many systems of interest, the external potential part is also time-independent, however, we keep its time dependence to account for those cases where the external potential changes with time, for

example, a time-dependent electric field. Later we will show that the final conclusion does not change whether V is time-dependent or not because $\langle \frac{\partial V(\boldsymbol{x},t)}{\partial t} \rangle$ will get canceled.

Taking the time derivative of eq S29 and combining with eq S33, we have

$$\frac{\mathrm{d}}{\mathrm{d}t}\langle A(t)|\hat{T}|A(t)\rangle + \frac{\mathrm{d}}{\mathrm{d}t}\frac{\langle\hat{\boldsymbol{p}}\rangle^2}{2m} + \frac{\mathrm{d}}{\mathrm{d}t}\frac{\sigma_{\boldsymbol{p}}^2}{2m} = \langle\frac{\partial V(\boldsymbol{x},t)}{\partial t}\rangle - \frac{\mathrm{d}}{\mathrm{d}t}\langle\hat{V}\rangle. \tag{S34}$$

Using $\frac{\mathrm{d}}{\mathrm{d}t}\frac{\langle\hat{\boldsymbol{p}}\rangle^2}{2m} = \frac{\langle\hat{\boldsymbol{p}}\rangle}{m}\cdot\frac{\mathrm{d}\langle\hat{\boldsymbol{p}}\rangle}{\mathrm{d}t}$, we can move most terms to the right hand side of eq S34 and get

$$\frac{\langle\hat{\boldsymbol{p}}\rangle}{m}\cdot\frac{\mathrm{d}\langle\hat{\boldsymbol{p}}\rangle}{\mathrm{d}t} = \langle\frac{\partial V}{\partial t}\rangle - \frac{\mathrm{d}}{\mathrm{d}t}\langle A(t)|\hat{T}|A(t)\rangle - \frac{\mathrm{d}}{\mathrm{d}t}\langle A(t)|\hat{V}|A(t)\rangle - \frac{\mathrm{d}}{\mathrm{d}t}\frac{\sigma_{\boldsymbol{p}}^2}{2m} \tag{S35}$$

$$= \langle\frac{\partial V}{\partial t}\rangle - \frac{\mathrm{d}}{\mathrm{d}t}\langle A(t)|\hat{H}|A(t)\rangle - \frac{\mathrm{d}}{\mathrm{d}t}\frac{\sigma_{\boldsymbol{p}}^2}{2m}. \tag{S36}$$

The derivation up to here is exact with no approximation imposed. However, this equation for the $\mathrm{d}\boldsymbol{p}/\,\mathrm{d}t$ part is not practically useful as the time derivatives on the right-hand side are unknown.

S1.3 Constrained minimization approximation

In order to make eq S36 an equation of motion that can be practically used in molecular dynamics simulations, here we proceed with an approximation that builds a connection between quantum states and the classical phase space.

Conventionally, if the potential is slowly varying in space, the Ehrenfest theorem provides a connection between the classical Newtonian dynamics in phase space $(\boldsymbol{X}, \boldsymbol{P})$ and the evolution of quantum expectation position and momentum $(\langle\hat{\boldsymbol{x}}\rangle, \langle\hat{\boldsymbol{p}}\rangle)$. Here with the same goal of mapping quantum states with the classical phase space, we approximate the quantum state as the energy-minimized state for a given classical phase space point. That is, when the system is at a particular phase space point given by an expectation position and an expectation momentum, i.e., $(\langle\hat{\boldsymbol{x}}\rangle, \langle\hat{\boldsymbol{p}}\rangle) = (\boldsymbol{X}, \boldsymbol{P})$, we assume that quantum state $|\Psi\rangle$ always adapts to the energy-minimized state for that phase space point. This approximation is in

essence an adiabatic approximation.

Under this approximation, quantum state $|\Psi\rangle$ becomes an explicit function of $(\boldsymbol{X}, \boldsymbol{P})$ and an implicit function of time t, i.e., $|\Psi\rangle(\boldsymbol{X}(t), \boldsymbol{P}(t))$. At a particular phase space point $(\boldsymbol{X}(t), \boldsymbol{P}(t))$ that the system evolves to at time t, the state can be obtained with a constrained energy minimization procedure. We write the Lagrangian as

$$\mathcal{L} = \langle\psi|\hat{H}(t)|\psi\rangle + \boldsymbol{f} \cdot (\langle\psi|\hat{\boldsymbol{x}}|\psi\rangle - \boldsymbol{X}(t)) - \boldsymbol{v} \cdot (\langle\psi|\hat{\boldsymbol{p}}|\psi\rangle - \boldsymbol{P}(t)) - \tilde{E}(\langle\psi|\psi\rangle - 1). \tag{S37}$$

where $\boldsymbol{f}$ is the Lagrange multiplier associated with the expectation position, $\boldsymbol{v}$ is the Lagrange multiplier associated with the expectation momentum, and $\tilde{E}$ is the Lagrange multiplier associated with the wave function normalization. We can further express the Lagrangian in terms of A and S, according to eqs S7 and S26:

$$\begin{aligned}
\mathcal{L} &= \langle\psi|\hat{T} + \hat{V}|\psi\rangle + \boldsymbol{f} \cdot (\langle A|\hat{\boldsymbol{x}}|A\rangle - \boldsymbol{X}(t)) \\
&\quad - \boldsymbol{v} \cdot \left(\int \mathrm{d}\boldsymbol{x} A^2(\boldsymbol{x}) \nabla S(\boldsymbol{x}) - \boldsymbol{P}(t) \right) - \tilde{E}(\langle\psi|\psi\rangle - 1) \qquad \text{(S38)} \\
&= \langle A|\hat{V}|A\rangle + \langle A|\hat{T}|A\rangle + \frac{1}{2m} \int \mathrm{d}\boldsymbol{x} A^2(\boldsymbol{x}) [\nabla S(\boldsymbol{x})]^2 + \boldsymbol{f} \cdot (\langle A|\hat{\boldsymbol{x}}|A\rangle - \boldsymbol{X}(t)) \\
&\quad - \boldsymbol{v} \cdot \left(\int \mathrm{d}\boldsymbol{x} A^2(\boldsymbol{x}) \nabla S(\boldsymbol{x}) - \boldsymbol{P}(t) \right) - \tilde{E}(\langle A|A\rangle - 1) \qquad \text{(S39)} \\
&= \langle A|\hat{H}|A\rangle + \frac{1}{2m} \int \mathrm{d}\boldsymbol{x} A^2(\boldsymbol{x}) [\nabla S(\boldsymbol{x})]^2 + \boldsymbol{f} \cdot (\langle A|\hat{\boldsymbol{x}}|A\rangle - \boldsymbol{X}(t)) \\
&\quad - \boldsymbol{v} \cdot \left(\int \mathrm{d}\boldsymbol{x} A^2(\boldsymbol{x}) \nabla S(\boldsymbol{x}) - \boldsymbol{P}(t) \right) - \tilde{E}(\langle A|A\rangle - 1). \qquad \text{(S40)}
\end{aligned}$$

At the state that minimizes the energy, the Lagrangian should be stationary with respect to A, S, as well as all the Lagrange multipliers.

We first take the functional derivative with respect to S part,

$$\frac{\delta\mathcal{L}}{\delta[\nabla S]} = A^2(\boldsymbol{x}) \left[\frac{\nabla S(\boldsymbol{x})}{m} - \boldsymbol{v} \right], \tag{S41}$$

and when it equals to zero, we have

$$\nabla S(\boldsymbol{x}) = m\boldsymbol{v}. \tag{S42}$$

This result means that under the adiabatic approximation, the momentum field is trivially uniform. Thus, according to the definition of the observable momentum field variance

$$\sigma_{\boldsymbol{p}}^2 = \int \mathrm{d}\boldsymbol{x} A^2(\boldsymbol{x},t)[\nabla S(\boldsymbol{x},t)]^2 - \left[\int \mathrm{d}\boldsymbol{x} A^2(\boldsymbol{x},t)\nabla S(\boldsymbol{x},t)\right]^2 = (m\boldsymbol{v})^2 - (m\boldsymbol{v})^2 = 0. \tag{S43}$$

Then the requirement on momentum constraint gives

$$\begin{aligned} \boldsymbol{P}(t) &= \langle\hat{\boldsymbol{p}}\rangle(t) && \text{(S44)}\\ &= \int \mathrm{d}\boldsymbol{x} A^2(\boldsymbol{x},t)\nabla S(\boldsymbol{x},t) && \text{(S45)}\\ &= m\boldsymbol{v}, && \text{(S46)} \end{aligned}$$

which further leads to the solution of the lagrange multiplier $\boldsymbol{v}$

$$\boldsymbol{v} = \frac{\boldsymbol{P}(t)}{m}. \tag{S47}$$

It is nothing but the velocity. Thus the momentum field as well as the phase part of the wave function is analytically solved and it is uniformly being

$$\nabla S(\boldsymbol{x}) = \boldsymbol{P}(t). \tag{S48}$$

Next we take the functional derivative for amplitude A part:

$$\frac{\delta\mathcal{L}}{\delta A} = 2\hat{H}A + \frac{1}{m}A(\nabla S)^2 + 2\boldsymbol{f}\cdot\hat{\boldsymbol{x}}A - 2\boldsymbol{v}\cdot\nabla SA - 2\tilde{E}A. \tag{S49}$$

Making it zero leads to the eigenvalue equation

$$\left[\hat{H}(t) + \frac{(\nabla S)^2}{2m} + \boldsymbol{f}\cdot\hat{\boldsymbol{x}} - \boldsymbol{v}\cdot\nabla S\right]|A\rangle = \tilde{E}|A\rangle. \tag{S50}$$

Because by solving the phase part we have known that $\nabla S = \boldsymbol{P}$ and $\boldsymbol{v} = \boldsymbol{P}/m$, this eigenvalue equation can further reduce to

$$[\hat{H}(t) + \boldsymbol{f}\cdot\hat{\boldsymbol{x}}]|A\rangle = \left(\tilde{E} + \frac{\boldsymbol{P}^2}{2m}\right)|A\rangle. \tag{S51}$$

The eigenvalue $\tilde{E} + \boldsymbol{P}^2/2m$, eigenstate $|A\rangle$, and the Lagrange multiplier $\boldsymbol{f}$ can be solved under the expectation position and normalization constraints for $|A\rangle$. Note again that the momentum constraint part has been solved analytically above.

With the adiabatic approximation, the solution of A only depends on current position $\boldsymbol{X}$, therefore, A is an explicit function of $\boldsymbol{X}$ and an implicit function of time t. Thus, the variable dependence can be written as:

$$A(\boldsymbol{x}, t) = A(\boldsymbol{x}; \boldsymbol{X}(t)). \tag{S52}$$

Thus, with the adiabatic approximation, we apply the chain rule to eq S36 and obtain

$$\begin{aligned}
\frac{\langle\hat{\boldsymbol{p}}\rangle}{m}\cdot\frac{\mathrm{d}\langle\hat{\boldsymbol{p}}\rangle}{\mathrm{d}t} &\approx \langle\frac{\partial V}{\partial t}\rangle - \frac{\mathrm{d}}{\mathrm{d}t}\langle A(\boldsymbol{X}(t))|\hat{H}|A(\boldsymbol{X}(t))\rangle && \text{(S53)}\\
&= \langle\frac{\partial V}{\partial t}\rangle - \langle A(\boldsymbol{X}(t))|\frac{\partial}{\partial t}\hat{H}|A(\boldsymbol{X}(t))\rangle - \langle\frac{\mathrm{d}}{\mathrm{d}t}A(\boldsymbol{X}(t))|\hat{H}|A(\boldsymbol{X}(t))\rangle \\
&\quad - \langle A(\boldsymbol{X}(t))|\hat{H}|\frac{\mathrm{d}}{\mathrm{d}t}A(\boldsymbol{X}(t))\rangle && \text{(S54)}\\
&= \langle\frac{\partial V}{\partial t}\rangle - \langle\frac{\partial V}{\partial t}\rangle - \langle\frac{\mathrm{d}}{\mathrm{d}t}A(\boldsymbol{X}(t))|\hat{H}|A(\boldsymbol{X}(t))\rangle - \langle A(\boldsymbol{X}(t))|\hat{H}|\frac{\mathrm{d}}{\mathrm{d}t}A(\boldsymbol{X}(t))\rangle && \text{(S55)}\\
&= -\langle\frac{\mathrm{d}}{\mathrm{d}t}A(\boldsymbol{X}(t))|\hat{H}|A(\boldsymbol{X}(t))\rangle - \langle A(\boldsymbol{X}(t))|\hat{H}|\frac{\mathrm{d}}{\mathrm{d}t}A(\boldsymbol{X}(t))\rangle && \text{(S56)}\\
&= -\frac{\mathrm{d}\boldsymbol{X}(t)}{\mathrm{d}t}\cdot[\langle\nabla_{\boldsymbol{X}}A|\hat{H}|A\rangle + \langle A|\hat{H}|\nabla_{\boldsymbol{X}}A\rangle] && \text{(S57)}\\
&= -\frac{\langle\hat{\boldsymbol{p}}\rangle}{m}\cdot\nabla_{\boldsymbol{X}}\langle A|\hat{H}|A\rangle. && \text{(S58)}
\end{aligned}$$

Note that $\hat{H}$ is dependent on $\boldsymbol{x}$, but it has no dependence on expectation position $\boldsymbol{X}$. Another interesting thing is that $\langle \frac{\partial V}{\partial t} \rangle$ gets canceled and does not explicitly show in the final result. Finally, according to classical mechanics, it is natural to assume that the change of $\langle \hat{\boldsymbol{p}} \rangle$ should have an opposite direction to the energy gradient term ($\nabla_{\boldsymbol{X}} \langle A|\hat{H}|A\rangle$), therefore, the common prefactor $|\langle \hat{\boldsymbol{p}} \rangle|/m$ can be dropped, and we arrive at the final expression

$$\frac{\mathrm{d}\langle \hat{\boldsymbol{p}} \rangle}{\mathrm{d}t} \approx -\nabla_{\boldsymbol{X}} \langle A|\hat{H}|A\rangle. \tag{S59}$$

This equation is simple and elegant, but we note that it should not be surprising to see this result because this equation essentially allows the energy transfer between observable kinetic energy and effective potential energy (including both regular potential energy and zero-point energy) with a conservation of total energy.

Equations S19 and S59 together make the equations of motion for CMES-MD.

S2 Generalization to multiple particles

Here we generalize the CMES-MD idea to the multi-particle case. The idea is completely the same as the section above but with slightly more tedious derivations.

Assume now we have N particles that are distinguishable (Note: we have to assume them to be distinguishable because if they are indistinguishable, the positions for each individual particles cannot be defined), and the potential energy surface $V(\boldsymbol{x}_1, \cdots, \boldsymbol{x}_N)$ is also known. The total wave function for these N particles should be a correlated form, but here we use a mean-field approximation and write the total nuclear wave function as a Hartree product:

$$\Psi(\boldsymbol{x}_1, \cdots, \boldsymbol{x}_N, t) = \psi_1(\boldsymbol{x}_1, t) \cdots \psi_N(\boldsymbol{x}_N, t). \tag{S60}$$

Each wave function ψ_i has its polar representation:

$$\psi_i(\boldsymbol{x}_i, t) = A_i(\boldsymbol{x}_i, t) \exp\left(\frac{\mathrm{i}}{\hbar} S(\boldsymbol{x}_i, t)\right). \tag{S61}$$

Their positions and momenta are

$$\begin{aligned}
\langle \hat{\boldsymbol{x}}_i \rangle(t) &= \int \mathrm{d}\boldsymbol{x}_1 \cdots \mathrm{d}\boldsymbol{x}_N |\Psi(\boldsymbol{x}_1, \cdots, \boldsymbol{x}_N, t)|^2 \boldsymbol{x}_i && \text{(S62)} \\
&= \int \mathrm{d}\boldsymbol{x}_1 \cdots \mathrm{d}\boldsymbol{x}_{j\neq i} \cdots \mathrm{d}\boldsymbol{x}_N A_1^2(\boldsymbol{x}_1, t) \cdots A_{j\neq i}^2(\boldsymbol{x}_{j\neq i}, t) \cdots A_N^2(\boldsymbol{x}_N, t) \int \mathrm{d}\boldsymbol{x}_i A_i^2(\boldsymbol{x}_i, t) \boldsymbol{x}_i && \text{(S63)} \\
&= \int \mathrm{d}\boldsymbol{x}_i A_i^2(\boldsymbol{x}_i, t) \boldsymbol{x}_i, && \text{(S64)}
\end{aligned}$$

$$\begin{aligned}
\langle \hat{\boldsymbol{p}}_i \rangle(t) &= -\mathrm{i}\hbar \int \mathrm{d}\boldsymbol{x}_1 \cdots \mathrm{d}\boldsymbol{x}_N \Psi^*(\boldsymbol{x}_1, \cdots, \boldsymbol{x}_N, t) \nabla_i \Psi(\boldsymbol{x}_1, \cdots, \boldsymbol{x}_N, t) && \text{(S65)} \\
&= \int \mathrm{d}\boldsymbol{x}_1 \cdots \mathrm{d}\boldsymbol{x}_{j\neq i} \cdots \mathrm{d}\boldsymbol{x}_N A_1^2(\boldsymbol{x}_1, t) \cdots A_{j\neq i}^2(\boldsymbol{x}_{j\neq i}, t) \cdots A_N^2(\boldsymbol{x}_N, t) \times \\
&\quad \int \mathrm{d}\boldsymbol{x}_i A_i^2(\boldsymbol{x}_i, t) \nabla_i S_i(\boldsymbol{x}_i, t) && \text{(S66)} \\
&= \int \mathrm{d}\boldsymbol{x}_i A_i^2(\boldsymbol{x}_i, t) \nabla_i S_i(\boldsymbol{x}_i, t). && \text{(S67)}
\end{aligned}$$

The total kinetic energy is

$$\begin{aligned}
\langle \hat{T} \rangle(t) &= \sum_i^N \langle \hat{T}_i \rangle(t) && \text{(S68)} \\
&= \sum_i^N \frac{\langle \hat{\boldsymbol{p}}_i^2 \rangle(t)}{2m_i} && \text{(S69)} \\
&= \sum_i^N -\frac{\hbar^2}{2m_i} \int \mathrm{d}\boldsymbol{x}_1 \cdots \mathrm{d}\boldsymbol{x}_N \Psi^*(\boldsymbol{x}_1, \cdots, \boldsymbol{x}_N, t) \nabla_i^2 \Psi(\boldsymbol{x}_1, \cdots, \boldsymbol{x}_N, t) && \text{(S70)} \\
&= \sum_i^N \frac{\hbar^2}{2m_i} \int \mathrm{d}\boldsymbol{x}_i [\nabla_i \psi_i^*(\boldsymbol{x}_i, t)] \cdot [\nabla_i \psi_i(\boldsymbol{x}_i, t)] && \text{(S71)}
\end{aligned}$$

$$= \sum_i^N \int \mathrm{d}\boldsymbol{x}_i A_i(\boldsymbol{x}_i,t) \frac{(-\mathrm{i}\hbar\nabla_i)^2}{2m_i} A_i(\boldsymbol{x}_i,t) + \frac{1}{2m_i}\int \mathrm{d}\boldsymbol{x}_i A_i^2(\boldsymbol{x}_i,t)[\nabla_i S_i(\boldsymbol{x}_i,t)]^2 \tag{S72}$$

$$= \sum_i^N \langle A_i(t)|\hat{T}_i|A_i(t)\rangle + \frac{\langle\hat{\boldsymbol{p}}_i\rangle^2(t)}{2m_i} + \frac{\sigma^2_{\boldsymbol{p}_i}(t)}{2m_i}. \tag{S73}$$

Similar to the single-particle case, we have the time derivative of energy identity:

$$\frac{\mathrm{d}}{\mathrm{d}t}\langle\hat{T}\rangle = \frac{\mathrm{d}}{\mathrm{d}t}\langle\hat{H}\rangle - \frac{\mathrm{d}}{\mathrm{d}t}\langle\hat{V}\rangle = \langle\frac{\partial V(\boldsymbol{x}_1,\cdots,\boldsymbol{x}_N,t)}{\partial t}\rangle - \frac{\mathrm{d}}{\mathrm{d}t}\langle\hat{V}(\boldsymbol{x}_1,\cdots,\boldsymbol{x}_N,t)\rangle. \tag{S74}$$

It further gives

$$\sum_i^N \frac{\langle\hat{\boldsymbol{p}}_i\rangle}{m_i}\cdot\frac{\mathrm{d}\langle\hat{\boldsymbol{p}}_i\rangle}{\mathrm{d}t} = \langle\frac{\partial V(\boldsymbol{x}_1,\cdots,\boldsymbol{x}_N,t)}{\partial t}\rangle - \frac{\mathrm{d}}{\mathrm{d}t}\langle\hat{V}(\boldsymbol{x}_1,\cdots,\boldsymbol{x}_N,t)\rangle -$$
$$\sum_i^N\left\{\frac{\mathrm{d}}{\mathrm{d}t}\langle A_i(t)|\hat{T}_i|A_i(t)\rangle + \frac{\mathrm{d}}{\mathrm{d}t}\frac{\sigma^2_{\boldsymbol{p}_i}(t)}{2m_i}\right\} \tag{S75}$$

$$= \langle\frac{\partial V(\boldsymbol{x}_1,\cdots,\boldsymbol{x}_N,t)}{\partial t}\rangle - \frac{\mathrm{d}}{\mathrm{d}t}\langle A_1\cdots A_N|\hat{T}+V(t)|A_1\cdots A_N\rangle - \sum_i^N\frac{\mathrm{d}}{\mathrm{d}t}\frac{\sigma^2_{\boldsymbol{p}_i}(t)}{2m_i}. \tag{S76}$$

The Lagrangian for the multi-particle case is

$$\mathcal{L} = \langle\Psi|\hat{H}(t)|\Psi\rangle + \sum_i^N \boldsymbol{f}_i\cdot(\langle\hat{\boldsymbol{x}}_i\rangle - \boldsymbol{X}_i(t)) - \boldsymbol{v}_i\cdot(\langle\hat{\boldsymbol{p}}_i\rangle - \boldsymbol{P}_i(t)) - \tilde{E}_i(\langle\psi_i|\psi_i\rangle - 1) \tag{S77}$$

$$= \langle A_1\cdots A_N|\hat{V}(t)|A_1\cdots A_N\rangle + \sum_i^N\langle A_i|\hat{T}_i|A_i\rangle + \frac{1}{2m_i}\int\mathrm{d}\boldsymbol{x}_i A_i^2(\boldsymbol{x}_i)[\nabla_i S_i(\boldsymbol{x}_i)]^2$$
$$+ \boldsymbol{f}_i\cdot(\langle A_i|\hat{\boldsymbol{x}}_i|A_i\rangle - \boldsymbol{X}_i(t)) - \boldsymbol{v}_i\cdot\left(\int\mathrm{d}\boldsymbol{x}_i A_i^2(\boldsymbol{x}_i)\nabla_i S_i(\boldsymbol{x}_i) - \boldsymbol{P}_i(t)\right) - \tilde{E}_i(\langle A_i|A_i\rangle - 1). \tag{S78}$$

Taking the functional derivative with respect to $\nabla_i S_i(\boldsymbol{x}_i)$ gives

$$\frac{\delta\mathcal{L}}{\delta[\nabla_i S_i]} = A_i^2(\boldsymbol{x}_i)\left[\frac{\nabla_i S_i(\boldsymbol{x}_i)}{m_i} - \boldsymbol{v}_i\right]. \tag{S79}$$

Making it zero leads to the solution

$$\nabla_i S_i(\boldsymbol{x}_i) = m_i \boldsymbol{v}_i = \boldsymbol{P}_i(t), \tag{S80}$$

which also makes each individual $\sigma^2_{\boldsymbol{p}_i}$ zero.

Taking the functional derivative with respect to $A_i(\boldsymbol{x}_i)$ gives

$$\begin{aligned}\frac{\delta \mathcal{L}}{\delta A_i} &= 2A_i \int \mathrm{d}\boldsymbol{x}_1 \cdots \mathrm{d}\boldsymbol{x}_{j\neq i} \cdots \mathrm{d}\boldsymbol{x}_N A_1^2(\boldsymbol{x}_1) \cdots A_{j\neq i}^2(\boldsymbol{x}_{j\neq i}) \cdots A_N^2(\boldsymbol{x}_N) V(\boldsymbol{x}_1, \cdots, \boldsymbol{x}_N, t) \\ &\quad + 2\hat{T}_i A_i + \frac{1}{m_i} A_i (\nabla_i S_i)^2 + 2\boldsymbol{f}_i \cdot \hat{\boldsymbol{x}}_i A_i - 2\boldsymbol{v_i} \cdot \nabla_i S_i A_i - 2\tilde{E}_i A_i \qquad \text{(S81)} \\ &= 2V_i(\boldsymbol{x}_i, t) A_i + 2\hat{T}_i A_i + 2\boldsymbol{f}_i \cdot \hat{\boldsymbol{x}}_i A_i - 2\left(\tilde{E}_i + \frac{\boldsymbol{P}_i^2}{2m_i}\right) A_i, \qquad \text{(S82)}\end{aligned}$$

where V_i is the effective potential that particle i is experiencing:

$$V_i(\boldsymbol{x}_i, t) \equiv \int \mathrm{d}\boldsymbol{x}_1 \cdots \mathrm{d}\boldsymbol{x}_{j\neq i} \cdots \mathrm{d}\boldsymbol{x}_N A_1^2(\boldsymbol{x}_1) \cdots A_{j\neq i}^2(\boldsymbol{x}_{j\neq i}) \cdots A_N^2(\boldsymbol{x}_N) V(\boldsymbol{x}_1, \cdots, \boldsymbol{x}_N, t). \tag{S83}$$

Making eq S82 zero leads to the eigenvalue equation for A_i:

$$[\hat{T}_i + V_i(\boldsymbol{x}_i, t) + \boldsymbol{f}_i \cdot \boldsymbol{x}_i] A_i(\boldsymbol{x}_i) = \left(\tilde{E}_i + \frac{\boldsymbol{P}_i^2}{2m_i}\right) A_i(\boldsymbol{x}_i). \tag{S84}$$

There are N coupled eigenvalue equations with N position constraints. Different particles interact with each other under the mean-field approximation. Now A_i is an implicit function of the time t through the explicit dependence on each particle's position:

$$A_i(\boldsymbol{x}_i, t) = A_i(\boldsymbol{x}_i; \{\boldsymbol{X}_j(t)\}_{j=1,\cdots,N}). \tag{S85}$$

Note that the positions of all particles affect the solution of A_i.

Equation S76 transforms to

$$\sum_i^N \frac{\langle \hat{\boldsymbol{p}}_i \rangle}{m_i} \cdot \frac{\mathrm{d}\langle \hat{\boldsymbol{p}}_i \rangle}{\mathrm{d}t} \approx \langle \frac{\partial V(\boldsymbol{x}_1, \cdots, \boldsymbol{x}_N, t)}{\partial t} \rangle - \frac{\mathrm{d}}{\mathrm{d}t} \langle A_1 \cdots A_N | \hat{T} + V(t) | A_1 \cdots A_N \rangle \tag{S86}$$

$$= \langle \frac{\partial V(\boldsymbol{x}_1, \cdots, \boldsymbol{x}_N, t)}{\partial t} \rangle - \langle \frac{\partial V(\boldsymbol{x}_1, \cdots, \boldsymbol{x}_N, t)}{\partial t} \rangle \tag{S87}$$

$$- \sum_i^N \frac{\mathrm{d}\boldsymbol{X}_i}{\mathrm{d}t} \cdot [\langle \nabla_{\boldsymbol{X}_i} (A_1 \cdots A_N) | \hat{T} + V(t) | A_1 \cdots A_N \rangle +$$

$$\langle A_1 \cdots A_N | \hat{T} + V(t) | \nabla_{\boldsymbol{X}_i} (A_1 \cdots A_N) \rangle] \tag{S88}$$

$$= - \sum_i^N \frac{\langle \hat{\boldsymbol{p}}_i \rangle}{m_i} \cdot \nabla_{\boldsymbol{X}_i} \langle A_1 \cdots A_N | \hat{T} + V(t) | A_1 \cdots A_N \rangle. \tag{S89}$$

According to classical mechanics, it is natural to assume that the change of each $\langle \hat{\boldsymbol{p}} \rangle$ should have an opposite direction to the corresponding energy gradient term ($\nabla_{\boldsymbol{X}} \langle A | \hat{H} | A \rangle$), then the final result is

$$\frac{\mathrm{d}\langle \hat{\boldsymbol{p}}_i \rangle}{\mathrm{d}t} \approx -\nabla_{\boldsymbol{X}_i} \langle A_1 \cdots A_N | \hat{T} + V(t) | A_1 \cdots A_N \rangle. \tag{S90}$$

S3 Generalization to CNEO-MD

For model systems above, we did not deal with electronic states, and the Born-Oppenheimer potential energy surfaces are assumed known beforehand. For practical molecular systems, we will take the electronic part into consideration, which will lead to CNEO-MD.

The total Hamiltonian for a molecular system is

$$\hat{H} = \hat{T}_\mathrm{e} + \hat{T}_\mathrm{n} + \hat{V}_\mathrm{ee} + \hat{V}_\mathrm{nn} + \hat{V}_\mathrm{ne}, \tag{S91}$$

where each term represents electronic kinetic energy, nuclear kinetic energy, electron-electron interaction energy, nucleus-nucleus interaction energy and electron-nucleus interaction energy, respectively. Here for simplicity we ignore the time-dependent external potential but as shown in sections above, it will not affect the final conclusion.

With the multicomponent Kohn-Sham density functional theory, if nuclei are assumed distinguishable, the total wave function can be expressed as

$$|\Psi\rangle = |\phi_1 \cdots \phi_{N_\mathrm{e}}\rangle |\psi_1\rangle \cdots |\psi_{N_\mathrm{n}}\rangle. \tag{S92}$$

We can perform similar derivations as in the previous section: starting with the polar representation for nuclear parts ψ_i, the nuclear kinetic energy part $\langle T_\mathrm{n}\rangle$ will have an equation identical to eq S73. Without a time-dependent external field, eq S74 essentially reduces to the law of energy conservation:

$$\frac{\mathrm{d}}{\mathrm{d}t} E_\mathrm{tot}\left[\rho_\mathrm{e}, \{\psi_i\}_{i=1,\cdots,N_\mathrm{n}}\right] = 0. \tag{S93}$$

Within the multicomponent Kohn-Sham formalism, if we ignore the electron-nucleus correlation, the total energy can be divided into the purely electronic part, the nuclear kinetic energy part, the nucleus-nucleus interaction part, and the mean-field electron-nucleus interaction part:

$$E_\mathrm{tot}\left[\rho_\mathrm{e}, \{\psi_i\}_{i=1,\cdots,N_\mathrm{n}}\right] = E_\mathrm{e}\left[\rho_\mathrm{e}\right] + \langle T_\mathrm{n}\rangle + \langle V_\mathrm{nn}\rangle + \langle V_\mathrm{ne}\left[\rho_\mathrm{e}\right]\rangle, \tag{S94}$$

where the angular brackets represent expectation values taken with nuclear wave functions. Taking the time derivative gives

$$\frac{\mathrm{d}}{\mathrm{d}t}\langle T_\mathrm{n}\rangle = -\frac{\mathrm{d}}{\mathrm{d}t}\left\{E_\mathrm{e}\left[\rho_\mathrm{e}\right] + \langle V_\mathrm{nn}\rangle + \langle V_\mathrm{ne}\left[\rho_\mathrm{e}\right]\rangle\right\}, \tag{S95}$$

and

$$\sum_i^{N_\mathrm{n}} \frac{\langle \hat{\boldsymbol{p}}_i\rangle}{m_i} \cdot \frac{\mathrm{d}\langle \hat{\boldsymbol{p}}_i\rangle}{\mathrm{d}t} = -\frac{\mathrm{d}}{\mathrm{d}t}\left\{E_\mathrm{e}\left[\rho_\mathrm{e}\right] + \langle V_\mathrm{nn}\rangle + \langle V_\mathrm{ne}\left[\rho_\mathrm{e}\right]\rangle\right\} - \sum_i^{N_\mathrm{n}} \left\{\frac{\mathrm{d}}{\mathrm{d}t}\langle A_i(t)|\hat{T}_i|A_i(t)\rangle + \frac{\mathrm{d}}{\mathrm{d}t}\frac{\sigma^2_{\boldsymbol{p}_i}(t)}{2m_i}\right\}. \tag{S96}$$

Under the adiabatic approximation, the Lagrangian that is used to perform the con-

strained minimization is

$$\begin{aligned}\mathcal{L} &= E_{\mathrm{tot}}\left[\rho_{\mathrm{e}}, \{\psi_i\}_{i=1,\cdots,N_{\mathrm{n}}}\right] - \sum_{ij} \epsilon_{ij}(\langle\phi_i|\phi_j\rangle - \delta_{ij}) \\ &\quad + \sum_{i}^{N_{\mathrm{n}}} \boldsymbol{f}_i \cdot (\langle\hat{\boldsymbol{x}}_i\rangle - \boldsymbol{X}_i(t)) - \boldsymbol{v}_i \cdot (\langle\hat{\boldsymbol{p}}_i\rangle - \boldsymbol{P}_i(t)) - \tilde{E}_i(\langle\psi_i|\psi_i\rangle - 1) \qquad \text{(S97)} \\ &= E_{\mathrm{e}}\left[\rho_{\mathrm{e}}\right] - \sum_{ij} \epsilon_{ij}(\langle\phi_i|\phi_j\rangle - \delta_{ij}) + \langle A_1 \cdots A_N \left|V_{\mathrm{ne}}\left[\rho_{\mathrm{e}}\right]\right| A_1 \cdots A_N\rangle \\ &\quad + \langle A_1 \cdots A_N \left|\hat{V}_{\mathrm{nn}}\right| A_1 \cdots A_N\rangle + \sum_{i}^{N_{\mathrm{n}}} \langle A_i|\hat{T}_i|A_i\rangle + \frac{1}{2m_i}\int \mathrm{d}\boldsymbol{x}_i A_i^2(\boldsymbol{x}_i)[\nabla_i S_i(\boldsymbol{x}_i)]^2 \\ &\quad + \boldsymbol{f}_i \cdot (\langle A_i|\hat{\boldsymbol{x}}_i|A_i\rangle - \boldsymbol{X}_i(t)) - \boldsymbol{v}_i \cdot \left(\int \mathrm{d}\boldsymbol{x}_i A_i^2(\boldsymbol{x}_i)\nabla_i S_i(\boldsymbol{x}_i) - \boldsymbol{P}_i(t)\right) - \tilde{E}_i(\langle A_i|A_i\rangle - 1). \qquad \text{(S98)}\end{aligned}$$

Similarly, we will have simple solutions to the nuclear phase part $\nabla_i S_i(\boldsymbol{x}_i)$ and the nuclear amplitude part needs to satisfy

$$[\hat{T}_i + V_i(\boldsymbol{x}_i) + \boldsymbol{f}_i \cdot \boldsymbol{x}_i]A_i(\boldsymbol{x}_i) = \left(\tilde{E}_i + \frac{\boldsymbol{P}_i^2}{2m_i}\right) A_i(\boldsymbol{x}_i), \qquad \text{(S99)}$$

where

$$V_i(\boldsymbol{x}_i) = V_{\mathrm{ne}}\left[\rho_{\mathrm{e}}\right](\boldsymbol{x}_i) + V_{\mathrm{nn}}\left[\{\rho_{\mathrm{n},j}\}_{j\neq i}\right](\boldsymbol{x}_i). \qquad \text{(S100)}$$

In addition to the nuclear part, the Lagrangian also needs to be stationary with respect to electronic orbital variations, which gives the electronic part of multicomponent Kohn-Sham equations:

$$\left\{\hat{T}_{\mathrm{e}} + U\left[\rho_{\mathrm{e}}\right] + V_{\mathrm{xc}}\left[\rho_{\mathrm{e}}\right] + V_{\mathrm{ne}}\left[\{\rho_{\mathrm{n}}\}\right]\right\}\phi_i = \epsilon_i\phi_i. \qquad \text{(S101)}$$

The electronic and nuclear Kohn-Sham equations are coupled with each other and need to be solved self-consistently. This set of constrained multicomponent Kohn-Sham equations is nothing but the CNEO-DFT equations, which has been developed in our group.

Similar to the derivations in above sections, the equation of motion for the observable

momentum part can be written as

$$\sum_{i}^{N_\mathrm{n}} \frac{\langle \hat{\boldsymbol{p}}_i \rangle}{m_i} \cdot \frac{\mathrm{d}\langle \hat{\boldsymbol{p}}_i \rangle}{\mathrm{d}t} \approx -\frac{\mathrm{d}}{\mathrm{d}t} \left\{ E_\mathrm{e}\left[\rho_\mathrm{e}\right] + \langle A_1 \cdots A_N \left| \hat{T} + \hat{V}_\mathrm{nn} + V_\mathrm{ne}\left[\rho_\mathrm{e}\right] \right| A_1 \cdots A_N \rangle \right\} \tag{S102}$$

$$= -\frac{\mathrm{d}}{\mathrm{d}t} E_\mathrm{tot}\left[\rho_\mathrm{e}, \{\rho_{\mathrm{n},i}\}_{i=1,\cdots,N_\mathrm{n}}\right] \tag{S103}$$

$$= -\sum_{i}^{N_\mathrm{n}} \frac{\mathrm{d}\boldsymbol{X}_i}{\mathrm{d}t} \cdot \nabla_{\boldsymbol{X}_i} E_\mathrm{tot}\left[\rho_\mathrm{e}, \{\rho_{\mathrm{n},i}\}_{i=1,\cdots,N_\mathrm{n}}\right] \tag{S104}$$

$$= -\sum_{i}^{N_\mathrm{n}} \frac{\langle \hat{\boldsymbol{p}}_i \rangle}{m_i} \cdot \nabla_{\boldsymbol{X}_i} E_\mathrm{tot}\left[\rho_\mathrm{e}, \{\rho_{\mathrm{n},i}\}_{i=1,\cdots,N_\mathrm{n}}\right]. \tag{S105}$$

Following the same arguments on classical mechanics, we have

$$\frac{\mathrm{d}\langle \hat{\boldsymbol{p}}_i \rangle}{\mathrm{d}t} \approx -\nabla_{\boldsymbol{X}_i} E_\mathrm{tot}\left[\rho_\mathrm{e}, \{\rho_{\mathrm{n},i}\}_{i=1,\cdots,N_\mathrm{n}}\right]. \tag{S106}$$

This result means that when both electronic and nuclear parts are explicitly taken into consideration, the whole CMES-MD derivation generalizes to CNEO-MD.

S4 Numerical validation of the adiabatic wave function propagation

In this section, we compare the adiabatic wave function propagation with exact quantum dynamics to test the quality of the adiabatic approximation. We used the same ^{16}O^{1}H Morse oscillator that was presented in the manuscript for this test. The initial wave packet is set to

$$\psi(x, t=0) = A_\mathrm{gs}(x) \exp\left(\mathrm{i}\frac{p_0 x}{\hbar}\right), \tag{S107}$$

where amplitude part A_gs is set to the ground state wave function of the Morse potential, and key component of the phase part p_0 is chosen such that the initial kinetic energy is equal

to $k_{\mathrm{B}} \times 300\,\mathrm{K}$:

$$\frac{p_0^2}{2m} = k_{\mathrm{B}} \times 300\,\mathrm{K}. \tag{S108}$$

Here m is the reduced mass of $^{16}\mathrm{O}^{1}\mathrm{H}$. p_0 is chosen to be positive, which means that the initial propagation stretches the bond. Because of the nonzero initial observable momentum, this total wave function is no longer at the ground state, and we simulate its propagation according to the time-dependent Schrödinger equation.

For the CMES-MD simulation, we also start with the ground state wave function and added the same momentum as in the quantum simulation, but instead of propagating according to time-dependent Schrödinger equation, the CMES-MD will propagate the position and momentum expectation values according to Newton's equations but with an underlying quantum wave function picture.

For comparison, we also performed classical MD simulations, it starts with a point charge at the bottom of the classical potential energy surface (PES), we also give it the same initial momentum as the other two simulations.

The (expectation) positions and (expectation) velocities as functions of time are plotted in Figure S1. Note that CMES and classical PES reach their individual energy minimum at different bond lengths and therefore initial positions for CMES-MD and classical MD are different. We can see that CMES-MD performs much better than classical MD with a very good overlap with the quantum reference.

Next, we directly compare the wave function overlaps. Here two possible definitions for the overlap are used:

1. Total wave function overlap, which is defined as

$$I_{\mathrm{tot}}(t) = \left| \int \mathrm{d}x \psi^*(x,t) A_{\mathrm{CMES}}(x; X(t)) \exp\left(\mathrm{i}\frac{mv(t)x}{\hbar}\right) \right|, \tag{S109}$$

   where $\psi(x,t)$ is the wave function according to the quantum dynamics propagation, and $A_{\mathrm{CMES}}(x; X(t)) \exp(\mathrm{i}\frac{mv(t)x}{\hbar})$ is the wave function that is behind the CMES-MD

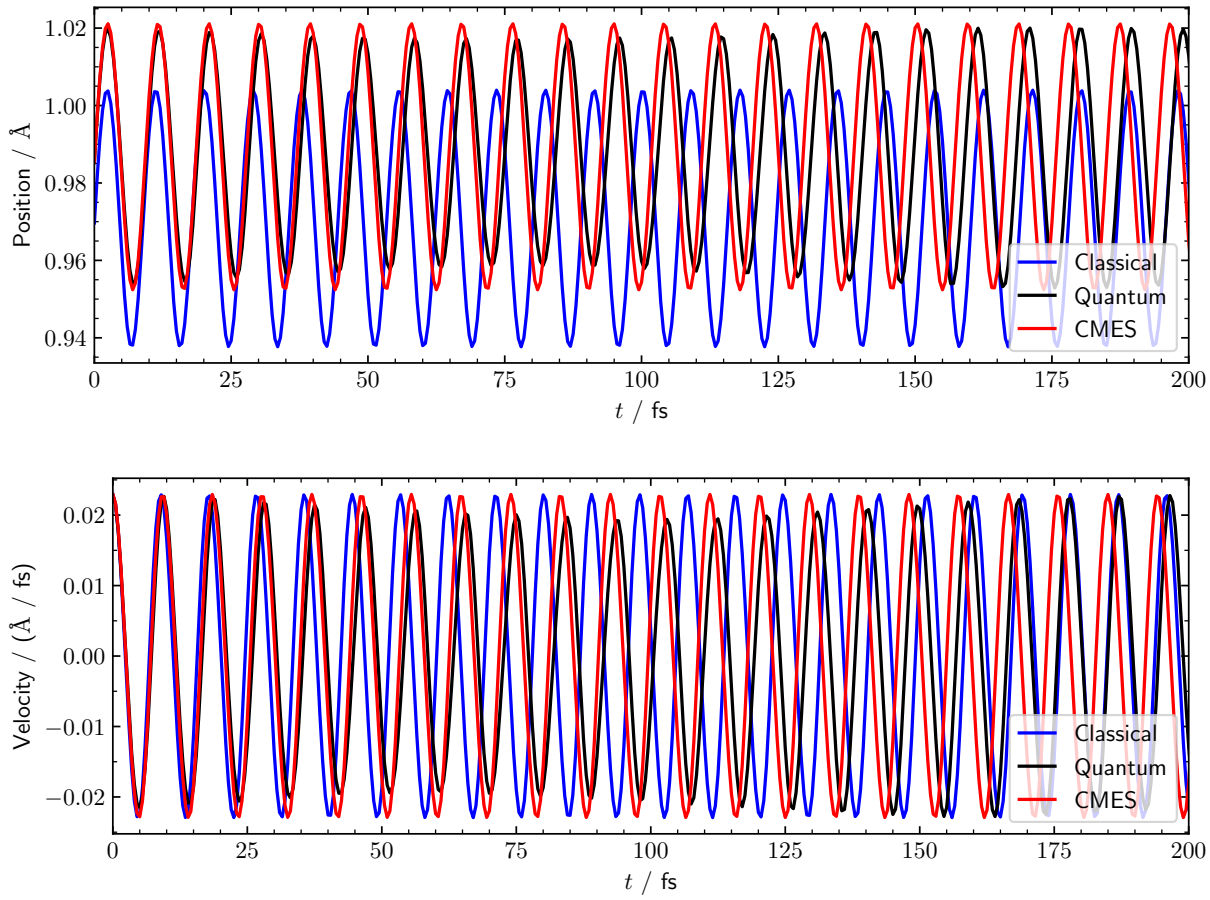


Figure S1: Trajectories from CMES-MD, classical MD and expectation values of quantum dynamics for the Morse oscillator.

with $X(t)$ being the expectation position and $v(t)$ being the expectation velocity.

2. Amplitude overlap:

$$I_{\text{amp}}(t) = \left| \int \mathrm{d}x A_{\text{QD}}(x,t) A_{\text{CMES}}(x; X(t)) \right|, \tag{S110}$$

where the quantum amplitude is from

$$A_{\text{QD}}(x,t) = \sqrt{|\psi(x,t)|^2}. \tag{S111}$$

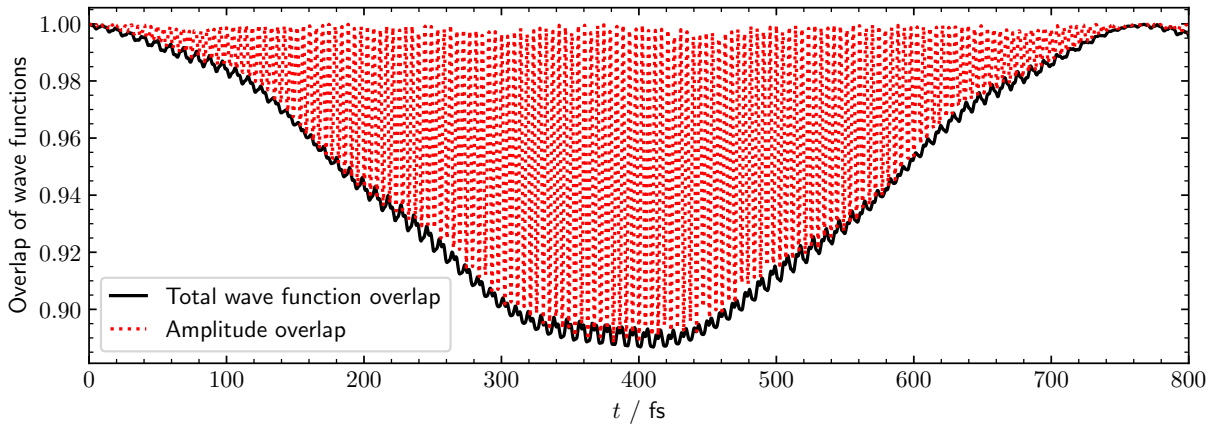


Figure S2: Overlap between the exact time-dependent wave function and CMES adiabatic wave functions for the Morse oscillator.

We can see from Figure S2 that, the total wave function overlap gradually decreases from 1 to around 0.89 in the first 400 fs, and then it increases in the next 400 fs due to a large period of quantum dynamics. We note that although 0.89 still seems a big overlap, it already means the physical picture is no longer right in this system. If we consider an overlap larger than 0.98 to be reasonably good, then in the short time scale of 100 fs, the adiabatic approximation works relatively well, and in a longer time scale, it cannot match quantum dynamics anymore. The amplitude overlap roughly describes how good the nuclear density is, and we can see that it oscillates between approximately 1 (indicating that the wave packet

positions are roughly the same and most errors are in momentum) and the value of the total wave function overlap (indicating that most errors lie in the wave packet description in the real space).

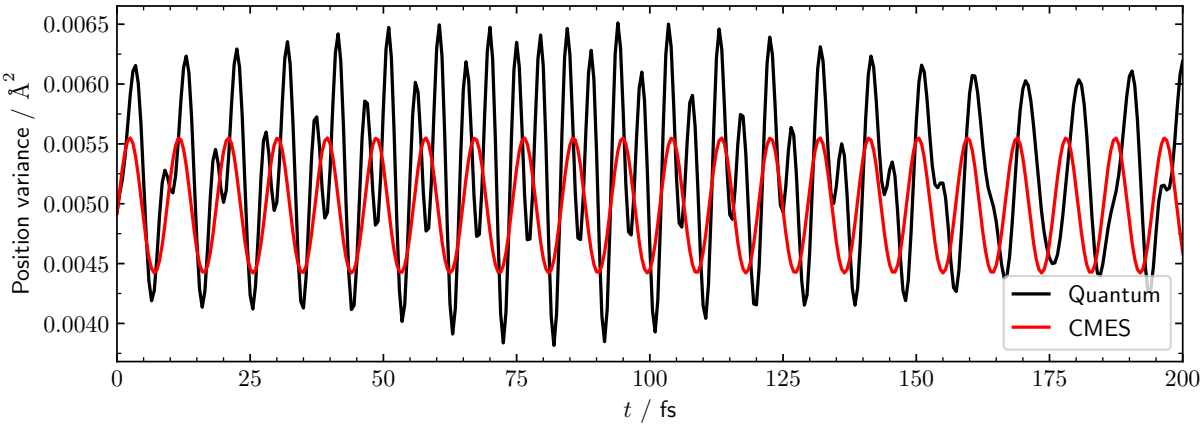


Figure S3: Position variances of the wave functions from CMES-MD and quantum dynamics for the Morse oscillator.

Then we investigate a more sensitive property: the variance of position. It roughly tells how delocalized the wave function is and is heavily influenced by quantum interferences. Now we can see in Figure S3 that even within the first 100 fs, the adiabatic CMES-MD is already much different from quantum dynamics with an oversimplified dynamics picture and no interference, which is not surprising considering the classical treatment as well as the adiabatic approximation.

In summary, CMES-MD can approximate quantum dynamics in a relatively short time scale, but it can be quite different from the quantum dynamics in a longer time scale.

References

(1) De Broglie, L. Sur la possibilité de relier les phénomenes d'interférence et de diffractiona la théorie des quanta de lumiere. *Comptes Rendus* **1926**, *183*, 447–448.

(2) De Broglie, L. La structure atomique de la matière et du rayonnement et la Mécanique ondulatoire. *CR Acad. Sci. Paris* **1927**, *184*, 273–274.

(3) Madelung, E. Quantentheorie in hydrodynamischer Form. *Z. Physik* **1927**, *40*, 322–326.

(4) Bohm, D. A Suggested Interpretation of the Quantum Theory in Terms of "Hidden" Variables. I. *Phys. Rev.* **1952**, *85*, 166–179.

(5) Bohm, D. A Suggested Interpretation of the Quantum Theory in Terms of "Hidden" Variables. II. *Phys. Rev.* **1952**, *85*, 180–193.

(6) Schleich, W. P.; Greenberger, D. M.; Kobe, D. H.; Scully, M. O. Schrödinger equation revisited. *Proc. Natl. Acad. Sci. U.S.A.* **2013**, *110*, 5374–5379.